

Improvements on Scalable Stochastic Bayesian Inference Methods for Multivariate Hawkes Process

Alex Ziyu Jiang¹ and Abel Rodriguez¹

¹Department of Statistics, University of Washington

Abstract

Multivariate Hawkes Processes (MHPs) are a class of point processes that can account for complex temporal dynamics among event sequences. In this work, we study the accuracy and computational efficiency of three classes of algorithms which, while widely used in the context of Bayesian inference, have rarely been applied in the context of MHPs: stochastic gradient expectation-maximization, stochastic gradient variational inference and stochastic gradient Langevin Monte Carlo. An important contribution of this paper is a novel approximation to the likelihood function that allows us to retain the computational advantages associated with conjugate settings while reducing approximation errors associated with the boundary effects. The comparisons are based on various simulated scenarios as well as an application to the study of risk dynamics in the Standard & Poor's 500 intraday index prices among its 11 sectors.

Keywords— Hawkes Processes; Stochastic Optimization; Variational inference; EM Algorithm; Langevin Monte Carlo; Bayesian Inference

1 Introduction

The multivariate Hawkes process (MHP) model (Hawkes, 1971; Liniger, 2009) is a class of temporal point process models that can capture complex time-event dynamics among multiple objects. Specifically, MHPs demonstrate the *self-* and *mutually-exciting* properties in multidimensional event sequences, where an event occurrence in a certain dimension leads to a higher likelihood of future events appearing in the same or other dimensions. This feature of the models makes MHPs attractive in a wide range of applications, including earth sciences (Ogata, 1988), finance (Bacry et al., 2015) and social media analysis (Rizou et al., 2017).

Computational methods for maximum likelihood inference in Hawkes process models include direct maximization of the likelihood function (e.g., see Ozaki, 1979) and the expectation-maximization (EM) algorithm (e.g., see Veen and Schoenberg, 2008 and Lewis and Mohler, 2011), as well as penalized least-squares estimation method of Bacry et al. (2020) and the variable selection-integrated maximum likelihood method of Bonnet et al. (2023) for sparse interaction settings. In the context of Bayesian inference, some of the algorithms that have been proposed include Markov Chain Monte Carlo algorithms (MCMC) (Rasmussen, 2013; Mohler, 2013; Holbrook et al., 2021, 2022; Deutsch and Ross, 2022), variational approximations (Xu and Zha, 2017; Malem-Shinitski et al., 2022; Sulem et al., 2022), sequential Monte Carlo (Linderman et al., 2017), and the maximum *a posteriori* probability estimation using the Expectation-Maximization algorithm (EM) (Zhang et al., 2018). In addition, theoretical guarantees for nonparametric Bayesian estimation methods of MHPs have been studied in Donnet et al. (2020) and Sulem et al. (2021). One key challenge associated with all these computational approaches is that they do not scale well to large datasets. Specifically, the double summation operation needed to carry out a single likelihood evaluation is typically of time complexity $\mathcal{O}(KN^2)$, where K is the number of dimensions and N is the number of total events. Even in situations where careful implementation can reduce the time complexity to $\mathcal{O}(KN)$ (e.g., for exponential excitation functions), the cost of this operation can be prohibitive for moderately large datasets. Furthermore, for methods that utilize the branching structure of MHPs, the space complexity is $\mathcal{O}(N^2)$ in all cases. An additional complication is that the calculation of the so-called “compensator” term in the likelihood function might limit our ability to exploit potential conjugacy in the model structure. Standard approximations to the compensator, which are well-justified when maximizing the full likelihood, can have a more serious impact when applied to small datasets, e.g., those arising in the context of algorithms that use subsets of the original data.

Algorithms inspired by stochastic optimization (Robbins and Monro, 1951) ideas, which approximate the gradient of the objective function through noisy versions evaluated on subsamples, offer an alternative for Bayesian inference on large datasets. Examples of such algorithms include stochastic gradient EM algorithms for finding the posterior mode of a model (e.g., see Chen et al., 2018), stochastic gradient variational algorithms (e.g., see Hoffman et al., 2013) and stochastic gradient

Hamiltonian Monte Carlo methods (e.g., see Nemeth and Fearnhead, 2021 and references therein). The use of stochastic gradient methods in the context of MHP models is, nonetheless, limited. Exceptions include Linderman and Adams (2015), who consider the use of stochastic gradient variational inference in the context of a discretized MHP, and Nickel and Le (2020), who discuss stochastic gradient methods to directly maximize the observed data likelihood.

In this paper, we discuss the efficient implementation of stochastic gradient EM, stochastic gradient variational approximations, and stochastic gradient Langevin diffusion methods in the context of parametric MHP models, and evaluate various aspects of their performance using both simulated and real datasets. A key contribution is an investigation of a novel approximation technique for the likelihood of the subsamples based on first-order Taylor expansion of the compensator term of the MHP models. We show that this novel approximation can lead to improvements in both point and interval estimation accuracy. For illustration purposes, we focus on intensity functions with exponential excitation functions. However, the insights gained from our experiments can be useful when working with other excitation functions that are proportional to density functions for which a conjugate prior on the unknown parameters is tractable.

Not only is the literature on stochastic gradient methods for Bayesian inference in MHP models limited, but the trade-offs between computational speed and accuracy are not well understood in this context. For *full-batch* methods (i.e., when using gradients based on the whole dataset rather than subsamples) Zhou et al. (2020) compares the estimation properties for EM, variational and random-walk MCMC algorithms. Our work extends this comparative evaluation to algorithms based on stochastic gradient methods. Additionally, we apply our methods to study the market risk dynamics in the Standard & Poor (S&P)'s 500 intraday index prices for its 11 sectors, using all three computation approaches. Our analysis suggests that the 11 sectors can be grouped into four categories. Price movements from sectors within the same category are more likely to be associated with each other, compared to sectors from different categories. Our analysis also shows that the effective range of the interactions between sectors is in the order of at most a few minutes.

2 Multivariate Hawkes process models

Let $\mathbf{X} = \{(t_i, d_i) : i = 1, \dots, n\}$ be a realization from a marked point process where $t_i \in \mathbb{R}^+$ represents the time at which the i -th event occurs and $d_i \in \{1, \dots, K\}$ is a mark that represents the dimension in which the event occurs. For example, t_i might represent the time at which user d_i makes a social media post, or the time at which the price of stock d_i drops below a certain threshold. Also, let n be the total number of events in the sequence and let n_k be the number of events in dimension k . Similarly, let $\mathcal{H}_t = \{(t_i, d_i) : t_i < t, t_i \in \mathbf{X}\}$ be the set of events that happened up until time t , and $N^{(k)}(t)$ be the number of events in dimension k that occurred on $[0, t]$. A sequence \mathbf{X} follows a multivariate Hawkes process if the conditional density function on dimension ℓ has the following form:

$$\lambda_\ell(t) \equiv \lim_{h \rightarrow 0} \frac{\mathbb{E}[N^{(\ell)}(t+h) - N^{(\ell)}(t) | \mathcal{H}_t]}{h} = \mu_\ell + \sum_{k=1}^K \sum_{t_i < t, d_i = k} \phi_{k,\ell}(t - t_i), \quad (1)$$

where $\mu_\ell > 0$ is the background intensity for dimension ℓ , and $\phi_{k,\ell}(\cdot) : \mathbf{R}^+ \rightarrow \mathbf{R}^+$ is the excitation function that controls how previous events in dimension ℓ affect the occurrence of new events in dimension k .

Common modeling choices for the excitation function include the exponential decay function where $\phi_{k,\ell}(\Delta) = \alpha_{k,\ell} \beta_{k,\ell} e^{-\beta_{k,\ell} \Delta}$ for $\Delta \geq 0$, and the power law decay function where $\phi_{k,\ell}(\Delta) = \frac{\alpha_{k,\ell} \beta_{k,\ell}}{(1 + \beta_{k,\ell} \Delta)^{1+\gamma_{k,\ell}}}$ for $\Delta \geq 0$. For illustration purposes, in this paper we focus on the exponential decay function. In that case, the parameter $\alpha_{k,\ell}$ controls the importance of events from dimension k on the appearance of events in dimension ℓ , and $\beta_{k,\ell}$ controls the magnitude of exponential decay of the instant change associated with a new event.

Let $\boldsymbol{\theta} = (\boldsymbol{\alpha}, \boldsymbol{\beta}, \boldsymbol{\mu})$ denote the vector of all model parameters. Using standard theory for point processes (e.g., see Daley and Vere-Jones, 2008), the observed log-likelihood associated with a Hawkes process can be written as

$$\begin{aligned} \mathcal{L}(\mathbf{X} | \boldsymbol{\alpha}, \boldsymbol{\beta}, \boldsymbol{\mu}) &= \sum_{\ell=1}^K \sum_{d_i=\ell} \log \lambda_\ell(t_i) - \sum_{\ell=1}^K \int_0^T \lambda_\ell(s) ds \\ &= \sum_{\ell=1}^K \sum_{d_i=\ell} \log \left(\mu_\ell + \sum_{k=1}^K \sum_{\substack{j < i \\ d_j=k, d_i=\ell}} \alpha_{k,\ell} \beta_{k,\ell} e^{-\beta_{k,\ell}(t_i - t_j)} \right) - \sum_{\ell=1}^K \mu_\ell T \\ &\quad - \sum_{k=1}^K \sum_{\ell=1}^K \alpha_{k,\ell} \left[n_k - \sum_{d_i=k} \exp(-\beta_{k,\ell}(T - t_i)) \right]. \end{aligned} \quad (2)$$

The MHP can also be obtained as a multidimensional Poisson cluster process in which each point is considered an “inmigrant” or an “offspring” (Hawkes and Oakes, 1974; Marsan and Lengline, 2008; Zhou et al., 2013; Rasmussen, 2013).

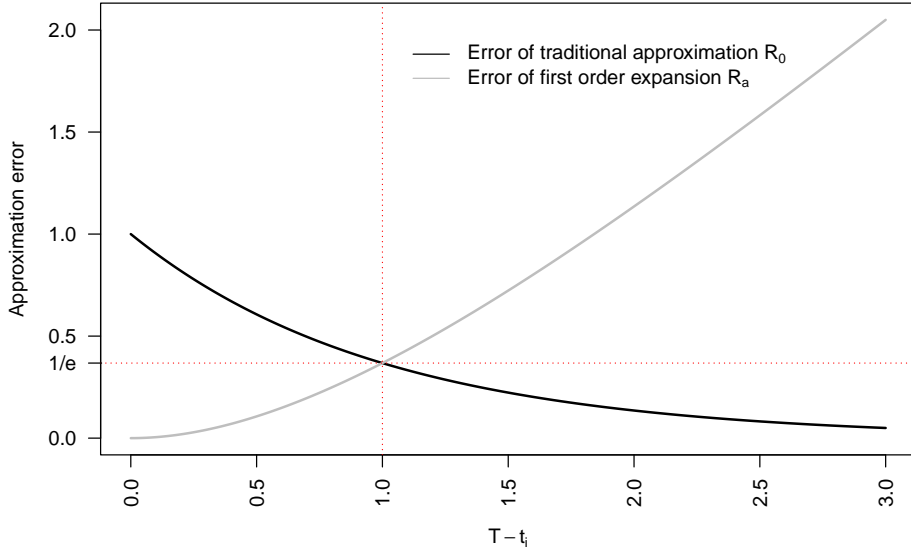


Figure 1: Trade off between approximation errors for the compensator for $\beta_{k,\ell} = 1$.

We use the lower-triangular $n \times n$ binary matrix \mathbf{B} to represent the latent branching structure of the events, where each row contains one and only one non-zero entry. For the strictly lower-triangular entries on the matrix, $B_{ij} = 1$ indicates that the i -th event can be viewed as an offspring of the j -th event. On the other hand, for the diagonal entries of the matrix, $B_{ii} = 1$ indicates that the i -th event is an immigrant. Each immigrant independently generates a cluster of offsprings that can further generate newer generations of offspring.

The branching structure, which is typically latent and unobservable, allows us to decouple the complex observed likelihood into factorizable terms and design simpler computational algorithms. The complete data log-likelihood, defined as the joint log-likelihood of the observed data and the branching structure \mathbf{B} , has the following form :

$$\begin{aligned} \mathcal{L}(\mathbf{X}, \mathbf{B} \mid \boldsymbol{\alpha}, \boldsymbol{\beta}, \boldsymbol{\mu}) = & \sum_{\ell=1}^K |I_{\ell}| \log \mu_{\ell} + \sum_{k=1}^K \sum_{\ell=1}^K \left[|O_{k,\ell}| (\log \alpha_{k,\ell} + \log \beta_{k,\ell}) - \beta_{k,\ell} \sum_{\substack{j < i \\ d_j=k, d_i=\ell}} B_{ij} (t_i - t_j) \right] \\ & - \sum_{\ell=1}^K \mu_{\ell} T - \sum_{k=1}^K \sum_{\ell=1}^K \alpha_{k,\ell} \left[n_k - \sum_{d_i=k} \exp(-\beta_{k,\ell} (T - t_i)) \right], \end{aligned} \quad (3)$$

where $|I_{\ell}| = \sum_{\substack{1 \leq i \leq n \\ d_i=\ell}} B_{ii}$ is the number of immigrants for dimension ℓ , and $|O_{k,\ell}| = \sum_{\substack{j < i \\ d_j=k, d_i=\ell}} B_{ij}$ is the number of descendants on dimension k that are an offspring of an event on dimension j .

2.1 Approximation for the data likelihood

The expressions for the observed and complete data likelihood in (2) and (3) share the same term

$$\Upsilon = \sum_{\ell=1}^K \int_0^T \lambda_{\ell}(s) ds = \sum_{\ell=1}^K \mu_{\ell} T + \sum_{k=1}^K \sum_{\ell=1}^K \alpha_{k,\ell} \left[\sum_{d_i=k} (1 - \exp\{-\beta_{k,\ell} (T - t_i)\}) \right]. \quad (4)$$

The integral $\int_0^T \lambda_{\ell}(s) ds$ is known as the compensator for the conditional density function $\lambda_{\ell}(t)$. The compensator guarantees that there are infinitely many ‘none events’ between observations on the finite temporal region $[0, T]$ (Mei and Eisner, 2017). The form of the compensator causes a number of computational challenges for designing scalable inference algorithms for MHP models (for a discussion see Lewis and Mohler, 2011, Schoenberg, 2013, Holbrook et al., 2021). A common approach used to avoid these challenges is to use the approximation technique introduced in Lewis and Mohler (2011):

$$\alpha_{k,\ell} [1 - \exp\{-\beta_{k,\ell} (T - t_i)\}] \approx \alpha_{k,\ell}, \quad (5)$$

for all $k, \ell = 1, \dots, K$. Clearly, this approximation is quite accurate for large values $T - t_i$. Therefore, if the process is stationary and T is “large” (ensuring that most observations are far away from T), the error $R_0(T - t_i) = \exp\{-\beta_{k,\ell}(T - t_i)\}$ is negligible for most i . However, for observations that are “close” to the boundary T , the approximation is quite poor. This will be an important consideration when designing algorithms for the MHP model that rely on subsamples because, in that setting, the equivalent quantity to T will be small and the edge effects cannot necessarily be assumed to be negligible.

To address this issue, we propose to use a different approximation for observations that are close to T . This alternative approximation is based on a first order Taylor expansion of the exponential function, so that

$$\alpha_{k,\ell} [1 - \exp\{-\beta_{k,\ell}(T - t_i)\}] \approx \alpha_{k,\ell} (1 - [1 - \beta_{k,\ell}(T - t_i)]) = \alpha_{k,\ell} \beta_{k,\ell}(T - t_i) \quad (6)$$

The error associated with this approximation is $R_a(T - t_i) = \sum_{n=2}^{\infty} \frac{(-\beta_{k,\ell}(T - t_i))^n}{n!} = \exp\{-\beta_{k,\ell}(T - t_i)\} - 1 + \beta_{k,\ell}(T - t_i)$. Hence, as opposed to (5), the approximation in (6) is accurate for small $T - t_i$. Furthermore, R_a is smaller than R_0 if and only if $T - t_i > 1/\beta_{k,\ell}$ (see Figure 1). This suggests dividing \mathbf{X} into two parts, based on whether the data points are observed within a predetermined threshold $(T - \delta, T]$ where $\delta = 1/\beta_{k,\ell}$, so that:

$$\alpha_{k,\ell} \left[\sum_{d_i=k} (1 - \exp\{-\beta_{k,\ell}(T - t_i)\}) \right] \approx \alpha_{k,\ell} \left[n_k - \sum_{0 \leq T - t_i < \delta, d_i=k} [1 - \beta_{k,\ell}(T - t_i)] \right], \quad (7)$$

for all $k, \ell = 1, \dots, K$. We call this the boundary-corrected approximation. One of its key advantages that it still allows us to exploit conjugacies in the definition of the model while providing a more accurate approximation for observations close to T . Please see Section 3 for additional details.

Note that, under our proposed approximation, the worst-case absolute error in the likelihood is bounded above by $n_{k,\ell}/e$. Furthermore, the approximation error is guaranteed to always be smaller than that from the original approximation in Lewis and Mohler (2011). Not only that, but it can also be shown that the average loss of information due to the approximation is negligible as $T \rightarrow \infty$ (see Appendix A).

2.2 Prior distributions

Bayesian inference for the MHP requires that we specify priors for the unknown parameters $(\boldsymbol{\alpha}, \boldsymbol{\beta}, \boldsymbol{\mu})$. For the baseline intensities we set

$$\mu_\ell \mid a_\ell, b_\ell \stackrel{i.i.d.}{\sim} \text{Gamma}(a_\ell, b_\ell),$$

which is conditionally conjugate given the branching structure \mathbf{B} . Similarly, under the exponential decay functions we use

$$\begin{aligned} \alpha_{k,\ell} \mid e_{k,\ell}, f_{k,\ell} &\stackrel{i.i.d.}{\sim} \text{Gamma}(e_{k,\ell}, f_{k,\ell}), \\ \beta_{k,\ell} \mid w_{k,\ell}, s_{k,\ell} &\stackrel{i.i.d.}{\sim} \text{Gamma}(w_{k,\ell}, s_{k,\ell}) \end{aligned}$$

which are also conditionally conjugate.

3 Computational methods

3.1 Preliminaries

In this section, we describe three stochastic gradient algorithms for MHP models based on the EM, variational inference and an Markov chain Monte Carlo algorithm based on Langevin dynamics algorithm, respectively. Before delving into the details of each algorithm, we discuss three issues that are relevant to the design of all of them.

The first issue refers to how to define the subsamples used to compute the gradient at each iteration. A common approach for regression models is to randomly select independent observations. However, the temporal dependence in event sequences makes this approach inappropriate for MHP models. Instead, our subsamples consist of all observations contained in the random interval $[T_0, T_0 + \kappa T]$, where we uniformly sample T_0 on $[0, (1 - \kappa)T]$ and $\kappa \in (0, 1]$ corresponds to the relative size of the subsample. Similar strategies have been applied to developing stochastic gradient variational algorithms for hidden Markov models (Foti et al., 2014) and stochastic block models (Gopalan et al., 2012).

The second issue relates to the selection of the learning rate ρ_r for the algorithms, which controls how fast the information from the stochastic gradient accumulates. It is well known (e.g., see Robbins and Monro, 1951) that the following conditions lead to convergence towards a local optima:

$$\sum_{r=1}^{\infty} \rho_r = \infty, \quad \sum_{r=1}^{\infty} \rho_r^2 < \infty. \quad (8)$$

In the following analysis, we apply the commonly used update schedule for ρ_r , outlined in Welling and Teh (2011):

$$\rho_r = \rho_0(r + \tau_1)^{-\tau_2}, \quad (9)$$

where ρ_0 is a common scaling factor, $\tau_2 \in (0.5, 1]$ is the forgetting rate that controls the exponential decay rate, and $\tau_1 \geq 0$ is the delay parameter that downweights early iterations. In our numerical experiments, we investigate the impact of specific choices of τ_1 and τ_2 on the results.

The third issue relates to the use of approximation techniques. We propose to use (7) to approximate the likelihood only for the stochastic gradient EM and variational inference algorithms since (conditional) conjugacy is important for developing these algorithms. In contrast, for stochastic gradient Langevin dynamics, we propose to use the exact likelihood in (2). For simplicity, we will refer to the algorithms with approximation as their ‘boundary-corrected’ versions, and we only show the update formula based on the ‘common approximation approach’ in this section. Additionally, we want to point out that the exponential decay function that we are using allows us to update $\boldsymbol{\mu}$ and $\boldsymbol{\alpha}$ using the exact likelihood formula, and we will only consider the approximation when we update $\boldsymbol{\beta}$.

3.2 Stochastic gradient EM algorithm for posterior mode finding

The expectation-maximization (EM) algorithm (Dempster et al., 1977) is an iterative maximization algorithm that is commonly used for latent variable models, especially in cases where knowledge of the latent variables simplifies the likelihood function. For Bayesian models, it can be used for maximum *a posteriori* probability estimation for the model parameters. Let \mathbf{X} be the observed dataset of size N , $\boldsymbol{\theta}$ be the set of model parameters to be estimated, and \mathbf{B} be the set of latent branching structure variables, and denote (\mathbf{X}, \mathbf{B}) as the complete dataset. We further assume that the distribution of the complete dataset belongs to the following exponential family:

$$l(\mathbf{X}, \mathbf{B} \mid \boldsymbol{\theta}) = A(\mathbf{X}, \mathbf{B}) \exp(\boldsymbol{\phi}(\boldsymbol{\theta})^\top \mathbf{s}(\mathbf{X}, \mathbf{B}) - \psi(\boldsymbol{\theta})), \quad (10)$$

where $\mathbf{s}(\mathbf{X}, \mathbf{B})$ is the vector of sufficient statistics for the complete data model and $\boldsymbol{\phi}(\boldsymbol{\theta})$ is the canonical form of the vector of parameters and $\boldsymbol{\phi}(\cdot)$ represents a one-to-one transformation.

In the context of Bayesian models, the EM algorithm can be used to obtain the maximum a posteriori (MAP) estimate (e.g., see Logothetis and Krishnamurthy, 1999). Starting from an initial guess of the model parameters $\boldsymbol{\theta}^{(0)}$, the EM algorithm alternatively carries out the following two steps until convergence:

- In the ‘E-step’, the algorithm estimates the “marginal” sufficient statistics based on the expected value $\hat{\mathbf{s}}^{(r)} := \mathbb{E}_{\mathbf{B} \mid \mathbf{X}, \boldsymbol{\theta}^{(r)}} [\mathbf{s}(\mathbf{X}, \mathbf{B})]$.
- In the ‘M-step’, the algorithm updates the model parameter as the maximizer of the Q function:

$$\boldsymbol{\theta}^{(r+1)} = \arg \min_{\boldsymbol{\theta}} \left[\boldsymbol{\phi}(\boldsymbol{\theta})^\top \hat{\mathbf{s}}^{(r)} + \log p(\boldsymbol{\theta}) \right].$$

where $p(\boldsymbol{\theta})$ denotes the prior on $\boldsymbol{\theta}$.

Note that the expectation calculation in the E-step update requires a pass through the whole dataset. As we discussed in the introduction, this can be challenging in very large datasets. The stochastic gradient EM (SGEM) algorithm (Cappe and Moulines, 2009) addresses this challenge by approximating the marginal sufficient statistics with an estimate based on randomly sampled mini-batches. We let $\mathbf{X}^{(r)}$ denote a subsample of size n (and respectively, we let $\mathbf{B}^{(r)}$ be the set of branching structure that corresponds to the selected subsample). For the stochastic E-step, the SGEM updates the estimated sufficient statistics $\hat{\mathbf{s}}^{(r+1)}$ as a linear combination of the previous update and a new estimate of the sufficient statistics based on the random subsample and the current model parameter:

$$\hat{\mathbf{s}}^{(r+1)} = (1 - \rho_r) \hat{\mathbf{s}}^{(r)} + \rho_r \kappa^{-1} \mathbb{E}_{\mathbf{B}^{(r+1)} \mid \mathbf{X}^{(r+1)}, \boldsymbol{\theta}^{(r)}} [\mathbf{s}(\mathbf{X}^{(r+1)}, \mathbf{B}^{(r+1)})].$$

where ρ_r is given in (9). Because of the way we select the subsamples, $\kappa^{-1} \mathbb{E}_{\mathbf{B}^{(r+1)} \mid \mathbf{X}^{(r+1)}, \boldsymbol{\theta}^{(r)}} [\mathbf{s}(\mathbf{X}^{(r+1)}, \mathbf{B}^{(r+1)})]$ is an unbiased estimate of the sufficient statistics of the model based on the whole dataset. In the following M-step, the SGEM algorithm maximizes the Q function

$$\boldsymbol{\theta}^{(r+1)} = \arg \max_{\boldsymbol{\theta}} \left[\boldsymbol{\phi}(\boldsymbol{\theta})^\top \hat{\mathbf{s}}^{(r+1)} + \log p(\boldsymbol{\theta}) \right].$$

In the case of the MHP model with exponential excitation functions, $\boldsymbol{\theta}^{(r)} = (\boldsymbol{\mu}^{(r)}, \boldsymbol{\alpha}^{(r)}, \boldsymbol{\beta}^{(r)})$ and the expectation in the E-step is computed with respect to the probabilities

$$p_{i,j}^{(r)} := p \left(\mathbf{B}_{i,j}^{(r)} = 1, \mathbf{B}_{i,-j}^{(r)} = 0 \mid \boldsymbol{\mu}^{(r)}, \boldsymbol{\alpha}^{(r)}, \boldsymbol{\beta}^{(r)}, \mathbf{X}^{(r)} \right) \propto \begin{cases} \mu_{d_i}^{(r)} & \text{if } j = i, \\ \alpha_{d_j, d_i}^{(r)} \beta_{d_j, d_i}^{(r)} \exp(-\beta_{d_j, d_i}^{(r)} (t_i - t_j)) & \text{if } j < i, \\ 0 & \text{if } j > i. \end{cases} \quad (11)$$

for $i = 2, \dots, n$, the negative subindex stands for all other possible except the one, and $p_{1,1}^{(r)} := 1$. Then, the vector of expected sufficient statistics of the complete data likelihood evaluated at iteration r

$$\left(s_{\mu,\ell,1}^{(r)}, s_{\mu,\ell,2}^{(r)}, s_{\alpha,k,\ell,1}^{(r)}, s_{\alpha,k,\ell,2}^{(r)}, s_{\beta,k,\ell,1}^{(r)}, s_{\beta,k,\ell,2}^{(r)} \right),$$

is updated as

$$\begin{aligned} s_{\mu,\ell,1}^{(r+1)} &= (1 - \rho_r) s_{\mu,\ell,1}^{(r)} + \rho_r \kappa^{-1} \sum_{d_i=\ell} p_{i,i}^{(r)}, \\ s_{\mu,\ell,2}^{(r+1)} &= T, \\ s_{\alpha,k,\ell,1}^{(r+1)} &= (1 - \rho_r) s_{\alpha,k,\ell,1}^{(r)} + \rho_r \kappa^{-1} \sum_{d_i=\ell} \sum_{\substack{d_j=k \\ j < i}} p_{i,j}^{(r)}, \\ s_{\alpha,k,\ell,2}^{(r+1)} &= (1 - \rho_r) s_{\alpha,k,\ell,1}^{(r)} + \kappa^{-1} \left(n_j^{(r)} - \sum_{d_j=k} \exp \left(-\beta_{k,l}^{(r)} (\kappa T - t_j) \right) \right), \\ s_{\beta,k,\ell,1}^{(r+1)} &= (1 - \rho_r) s_{\beta,k,\ell,1}^{(r)} + \rho_r \kappa^{-1} \sum_{d_i=l} \sum_{\substack{d_j=k \\ j < i}} p_{i,j}^{(r)} \\ s_{\beta,k,\ell,2}^{(r+1)} &= (1 - \rho_r) s_{\beta,k,\ell,2}^{(r)} + \rho_r \kappa^{-1} \sum_{d_i=l} \sum_{\substack{d_j=k \\ j < i}} p_{i,j}^{(r)} (t_i - t_j), \end{aligned}$$

where $n_j^{(r)}$ denotes the number of events on dimension j in $\mathbf{X}^{(r)}$. Finally, in the M-step, the value of the parameters is updated as:

$$\alpha_{k,\ell}^{(r+1)} = \frac{s_{\alpha,k,\ell,1}^{(r+1)} + e_{k,\ell} - 1}{s_{\alpha,k,\ell,2}^{(r+1)} + f_{k,\ell}}, \quad \beta_{k,\ell}^{(r+1)} = \frac{s_{\beta,k,\ell,1}^{(r+1)} + w_{k,\ell} - 1}{s_{\beta,k,\ell,2}^{(r+1)} + s_{k,\ell}}, \quad \mu_\ell^{(r)} = \frac{s_{\mu,\ell,1}^{(r+1)} + a_\ell - 1}{s_{\mu,\ell,2}^{(r+1)} + b_\ell}.$$

We repeat the steps above until the convergence criterion is reached.

3.3 Stochastic Gradient Variational Inference

Variational inference (Wainwright et al., 2008) is an approximate inference method that replaces the posterior distribution with an approximation that belongs to a tractable class. More specifically, the variational approximation $q_\eta(\boldsymbol{\theta}, \mathbf{B})$, $\eta \in H$ to the posterior distribution $p(\boldsymbol{\theta}, \mathbf{B} | \mathbf{X})$ is obtained through maximizing the evidence lower bound (ELBO), which is equivalent to setting

$$\eta = \arg \max_{\tilde{\eta} \in H} \mathbb{E}_{q_{\tilde{\eta}}} \log \left\{ \frac{p(\boldsymbol{\theta}, \mathbf{B}, \mathbf{X})}{q_{\tilde{\eta}}(\boldsymbol{\theta}, \mathbf{B})} \right\}. \quad (12)$$

The class of variational approximations most used in practice is the class of mean-field approximations (Bishop and Nasrabadi, 2006), where model parameters are taken to be independent from each other under the variational distribution, i.e., $q_\eta(\boldsymbol{\theta}, \mathbf{B}) = \prod_j q_{\eta_{\theta_j}}(\theta_j) \prod_i q_{\eta_{\mathbf{B}_i}}(\mathbf{B}_i)$. If both the full conditional posterior distributions and the corresponding variational distribution belong to the same exponential family, e.g., if

$$p(\theta_j | \boldsymbol{\theta}_{-j}, \mathbf{B}, \mathbf{X}) = A(\theta_j) \exp \{ \theta_j s_j(\boldsymbol{\theta}_{-j}, \mathbf{B}, \mathbf{X}) - \psi(\boldsymbol{\theta}_{-j}, \mathbf{X}) \}, \quad q_{\eta_{\theta_j}}(\theta_j) = A(\theta_j) \exp \{ \theta_j s_i(\boldsymbol{\eta}_{\theta_j}) - \psi(\boldsymbol{\eta}_{\theta_j}) \},$$

Blei and Jordan (2006) showed that the coordinate ascent algorithm for the mean-field variational inference updates the variational parameters by setting $\eta_{\theta_j}^{(r+1)} = \mathbb{E}_{q_{\eta^{(r)}}} [s_j(\boldsymbol{\theta}_{-j}, \mathbf{B}, \mathbf{X})]$. A similar result applies to the updates of the variational parameters $\eta_{\mathbf{B}_i}$.

Stochastic gradient variational inference (SGVI) (Hoffman et al., 2013) is a variant of variational inference that replaces the gradient computed over the whole sample with the one calculated over a random subsample $\mathbf{X}^{(r)}$ of size n selected during iteration r . Under conjugacy, SGVI then updates the vector $\boldsymbol{\eta}_{\mathbf{B}}$ in iteration r by setting

$$\eta_{\mathbf{B}_i^{(r)}}^{(r+1)} = \mathbb{E}_{q_{\eta^{(r)}}} \left[\tilde{s}_i(\mathbf{B}_{-i}^{(r)}, \boldsymbol{\theta}, \mathbf{X}^{(r)}) \right],$$

where $\tilde{s}_i(\mathbf{B}_{-i}^{(r)}, \boldsymbol{\theta}, \mathbf{X}^{(r)})$ is the sufficient statistics associated with the block \mathbf{B}_i , and $\boldsymbol{\eta}_{\boldsymbol{\theta}}$ through the recursion

$$\eta_{\theta_j}^{(r+1)} = (1 - \rho_r) \eta_{\theta_j}^{(r)} + \rho_r \hat{\eta}_{\theta_j}^{(r+1)},$$

where $\hat{\eta}_{\boldsymbol{\theta}_j}^{(r+1)} = \text{E}_{q_{\boldsymbol{\eta}}^{(r+1)}} \left[s_j(\boldsymbol{\theta}_{-j}, \mathbf{B}^{(r)}, \mathbf{X}^{(r)}) \right]$. In the specific case of the MHP with exponential excitation functions we have $\boldsymbol{\theta} = (\boldsymbol{\mu}, \boldsymbol{\alpha}, \boldsymbol{\beta})$, $\boldsymbol{\eta} = (\boldsymbol{\eta}_{\boldsymbol{\alpha}}, \boldsymbol{\eta}_{\boldsymbol{\beta}}, \boldsymbol{\eta}_{\boldsymbol{\mu}}, \boldsymbol{\eta}_{\mathbf{B}})$ and

$$q_{\boldsymbol{\eta}}(\boldsymbol{\alpha}, \boldsymbol{\beta}, \boldsymbol{\mu}, \mathbf{B}) = \prod_{i=1}^N q_{\boldsymbol{\eta}_{\mathbf{B}_i}}(\mathbf{B}_i) \prod_{k=1}^K q_{\boldsymbol{\eta}_{\boldsymbol{\mu}_k}}(\boldsymbol{\mu}_k) \prod_{j=1}^K \prod_{k=1}^K q_{\boldsymbol{\eta}_{\boldsymbol{\alpha}_{k,\ell}}}(\alpha_{k,\ell}) q_{\boldsymbol{\eta}_{\boldsymbol{\beta}_{k,\ell}}}(\beta_{k,\ell}),$$

where $\alpha_{k,\ell} \sim \text{Gamma}(\eta_{\alpha,k,\ell,1}, \eta_{\alpha,k,\ell,2})$, $\beta_{k,\ell} \sim \text{Gamma}(\eta_{\beta,k,\ell,1}, \eta_{\beta,k,\ell,2})$, $\mu_{\ell} \sim \text{Gamma}(\eta_{\mu,\ell,1}, \eta_{\mu,\ell,2})$, \mathbf{B}_i denotes the i -th row of the matrix \mathbf{B} , and \mathbf{B}_i follows a categorical distribution with parameter $\boldsymbol{\eta}_{\mathbf{B}_i}$. Hence, each iteration of the SGVI algorithm starts by updating the variational parameter for the local branching structure through the following formula:

$$\eta_{B_{ij}^{(r)}} \propto \begin{cases} \exp \left\{ \psi \left(\eta_{\mu, d_i, 1}^{(r)} \right) - \log \left(\eta_{\mu, d_i, 2}^{(r)} \right) \right\} & j = i \\ \exp \left\{ \Psi_{ij} - \log \left(\eta_{\alpha, d_j, d_i, 2}^{(r)} \right) - \log \left(\eta_{\beta, d_j, d_i, 2}^{(r)} \right) \right\} & j < i, \\ 0 & j > i, \end{cases}$$

where $\Psi_{ij} = \psi \left(\eta_{\alpha, d_j, d_i, 1}^{(r)} \right) + \psi \left(\eta_{\beta, d_j, d_i, 1}^{(r)} \right) - \frac{\eta_{\beta, d_j, d_i, 1}^{(r)}}{\eta_{\beta, d_j, d_i, 2}^{(r)}} \left(t_i^{(r)} - t_j^{(r)} \right)$. In this expression, $\psi(x) = \frac{d}{dx} \ln \Gamma(x)$ denotes the digamma function, and $(t_i^{(r)}, t_j^{(r)})$ represents the i -th and j -th event in $\mathbf{X}^{(r)}$. Then, we update the rest of the variational parameters as:

$$\begin{aligned} \eta_{\alpha_{k,\ell,1}}^{(r+1)} &= (1 - \rho_r) \eta_{\alpha_{k,\ell,1}}^{(r)} + \rho_r \left(\kappa^{-1} \sum_{d_i=\ell} \sum_{\substack{d_j=k \\ j < i}} \eta_{B_{ij}^{(r)}} + e_{k,\ell} \right), \\ \eta_{\alpha_{k,\ell,2}}^{(r+1)} &= (1 - \rho_r) \eta_{\alpha_{k,\ell,2}}^{(r)} + \rho_r \left(\kappa^{-1} \left(n_k^{(r)} - \sum_{d_j=k} \left(1 + \frac{\kappa T - t_j}{\eta_{\beta_{k,\ell,2}}^{(r+1)}} \right)^{-\eta_{\beta_{k,\ell,1}}^{(r+1)}} \right) + f_{k,\ell} \right), \\ \eta_{\beta_{k,\ell,1}}^{(r+1)} &= (1 - \rho_r) \eta_{\beta_{k,\ell,1}}^{(r)} + \rho_r \left(\kappa^{-1} \sum_{d_i=\ell} \sum_{\substack{d_j=k \\ j < i}} \eta_{B_{ij}^{(r)}} + r_{k,\ell} \right), \\ \eta_{\beta_{k,\ell,2}}^{(r+1)} &= (1 - \rho_r) \eta_{\beta_{k,\ell,2}}^{(r)} + \rho_r \left(\kappa^{-1} \sum_{d_i=\ell} \sum_{\substack{d_j=k \\ j < i}} \eta_{B_{ij}^{(r)}} (t_i^{(r)} - t_j^{(r)}) + s_{k,\ell} \right), \\ \eta_{\mu_{\ell,1}}^{(r+1)} &= (1 - \rho_r) \eta_{\mu_{\ell,1}}^{(r)} + \rho_r \left(\kappa^{-1} \sum_{d_i=\ell} \eta_{B_{ii}^{(r)}} + a_{\ell} \right), \\ \eta_{\mu_{\ell,2}}^{(r+1)} &= T + b_{\ell}. \end{aligned}$$

These updates are repeated until convergence.

3.4 Stochastic Gradient Langevin Dynamics

Unlike the previous two sections, here we focus on inference methods that are based on the observed data likelihood (2) instead of the complete data likelihood (3). Specifically, we consider simulation methods that rely on Langevin dynamics (LD) (Neal, 2011), a class of MCMC methods that are based on the discretization of a continuous-time stochastic process whose equilibrium distribution is the desired posterior distribution. Compared to simple random walk MCMC algorithms, LD algorithms explore the parameter space much more efficiently because they use information about the gradient of the likelihood to guide the direction of the random walk. In particular, LD methods propose new values for the parameter according to

$$\boldsymbol{\theta}^* = \boldsymbol{\theta}^{(r)} - \frac{\rho}{2} \nabla_{\boldsymbol{\theta}} U(\boldsymbol{\theta} \mid \mathbf{X})|_{\boldsymbol{\theta}=\boldsymbol{\theta}^{(r)}} + \sqrt{\rho} \epsilon_{r+1}, \quad (13)$$

where ρ is the step size used to discretize the Langevin diffusion, $U(\boldsymbol{\theta} \mid \mathbf{X}) = -\log p(\mathbf{X} \mid \boldsymbol{\theta}) - \log p(\boldsymbol{\theta})$ is the negative logarithm of the unnormalized posterior of interest, and ϵ_{r+1} is drawn from a standard multivariate normal distribution. If no discretization of the Langevin diffusion was involved, then this proposed value would come from the correct stationary

distribution. However, the introduction of the discretization means that a correction is required. Hence, values proposed according to (13) are accepted with probability

$$\min \left\{ 1, \frac{\exp \{-U(\boldsymbol{\theta}^* | \mathbf{X})\}}{\exp \{-U(\boldsymbol{\theta}^{(r)} | \mathbf{X})\}} \right\}. \quad (14)$$

If accepted, then $\boldsymbol{\theta}^{(r+1)} = \boldsymbol{\theta}^*$. Otherwise, $\boldsymbol{\theta}^{(r+1)} = \boldsymbol{\theta}^{(r)}$.

The stochastic gradient Langevin Dynamics (SGLD) algorithm (Welling and Teh, 2011; Chen et al., 2014) replaces the likelihood computed over the whole sample with (an appropriately rescaled) likelihood evaluated on a random subsample $\mathbf{X}^{(r)}$. SGLD also uses a decreasing stepsize ρ_r to construct the discretization of the Langevin diffusion in step r of the algorithm and ignores the correction step in (14). This leads to updates of the form

$$\boldsymbol{\theta}^{(r+1)} = \boldsymbol{\theta}^{(r)} - \frac{\rho_r}{2} \nabla_{\boldsymbol{\theta}} \tilde{U}(\boldsymbol{\theta} | \mathbf{X}^{(r)}) \Big|_{\boldsymbol{\theta}=\boldsymbol{\theta}^{(r)}} + \sqrt{\rho_r} \epsilon_{r+1}, \quad (15)$$

where $\tilde{U}(\boldsymbol{\theta} | \mathbf{X}^{(r)}) = \kappa^{-1} \log p(\mathbf{X}^{(r)} | \boldsymbol{\theta}) + \log p(\boldsymbol{\theta})$.

In the case of the MHP model with exponential excitation functions, we perform a logarithmic transformation on the model parameters before implementing the SGLD, so that $\boldsymbol{\xi}_{\alpha} = \log \boldsymbol{\alpha}$, $\boldsymbol{\xi}_{\beta} = \log \boldsymbol{\beta}$ and $\boldsymbol{\xi}_{\mu} = \log \boldsymbol{\mu}$. Then, the gradients become:

$$\begin{aligned} \nabla_{\xi_{\alpha_{k,\ell}}}^{(r)} U(\boldsymbol{\xi}) &= - \sum_{d_i=\ell} \frac{\alpha_{k,\ell}^{(r)} \beta_{k,\ell}^{(r)} \sum_{d_j=k, j < i} \exp \left(-\beta_{k,\ell}^{(r)} (t_i^{(r)} - t_j^{(r)}) \right)}{\mu_{\ell}^{(r)} + \alpha_{k,\ell}^{(r)} \beta_{k,\ell}^{(r)} \sum_{d_j=k, j < i} \exp \left(-\beta_{k,\ell}^{(r)} (t_i^{(r)} - t_j^{(r)}) \right)} \\ &\quad + \alpha_{k,\ell}^{(r)} \left(n_k^{(r)} - \sum_{d_j=k} \exp \left(-\beta_{k,\ell}^{(r)} (\kappa T - t_j) \right) + f_{k,\ell} \right) - e_{k,\ell}, \\ \nabla_{\xi_{\beta_{k,\ell}}}^{(r)} U(\boldsymbol{\xi}) &= - \sum_{d_i=\ell} \frac{\alpha_{k,\ell}^{(r)} \beta_{k,\ell}^{(r)} \sum_{d_j=k, j < i} \left(1 - \beta_{k,\ell}^{(r)} (t_i^{(r)} - t_j^{(r)}) \right) \exp \left(-\beta_{k,\ell}^{(r)} (t_i^{(r)} - t_j^{(r)}) \right)}{\mu_{\ell}^{(r)} + \alpha_{k,\ell}^{(r)} \beta_{k,\ell}^{(r)} \sum_{d_j=k, j < i} \exp \left(-\beta_{k,\ell}^{(r)} (t_i^{(r)} - t_j^{(r)}) \right)} \\ &\quad + \sum_{d_j=k} \alpha_{k,\ell}^{(r)} (\kappa T - t_j) \exp \left(-\beta_{k,\ell}^{(r)} (\kappa T - t_j) \right) - r_{k,\ell} + s_{k,\ell} \beta_{k,\ell}^{(r)}, \\ \nabla_{\xi_{\mu_{k,\ell}}}^{(r)} U(\boldsymbol{\xi}) &= - \sum_{d_i=\ell} \frac{\mu_{\ell}^{(r)}}{\mu_{\ell}^{(r)} + \alpha_{k,\ell}^{(r)} \beta_{k,\ell}^{(r)} \sum_{d_j=k, j < i} \exp \left(-\beta_{k,\ell}^{(r)} (t_i^{(r)} - t_j^{(r)}) \right)} + \mu_{\ell}^{(r)} (b_{\ell} + \kappa T) - a_{\ell}. \end{aligned}$$

Note that SGLD does not require approximating the observed data likelihood.

4 Simulation studies

In this section, we conduct a series of simulations to understand the performance of the algorithms with and without time budget constraints. Compared with small-scale learning problems, large-scale problems are subject to a qualitatively different tradeoffs involving the computational complexity of the underlying algorithm (Bottou and Bousquet, 2007), making evaluation under time constraints key. We also investigate the model fitting performance of all algorithms under different subsampling ratios.

4.1 Experimental setting

Data generation mechanism. For most of our experiments, data is generated from the multivariate Hawkes process model presented in section 2 with $K = 3$ dimensions and the following parameter settings:

$$\boldsymbol{\alpha} = \begin{bmatrix} 0.3 & 0.3 & 0.3 \\ 0.3 & 0.3 & 0.3 \\ 0.3 & 0.3 & 0.3 \end{bmatrix}, \quad \boldsymbol{\beta} = \begin{bmatrix} 4 & 4 & 4 \\ 4 & 4 & 4 \\ 4 & 4 & 4 \end{bmatrix}, \quad \boldsymbol{\mu} = \begin{bmatrix} 0.5 \\ 0.5 \\ 0.5 \end{bmatrix}.$$

In addition, for our last set of experiments, we also consider an alternative data generation mechanism for a 10-dimensional Hawkes processes with varying degrees of sparsity on the matrix $\boldsymbol{\alpha}$. More specifically, we let have $\mu_{\ell} = 0.1$, $\beta_{k,\ell} = 4$ for all $k, \ell = 1, \dots, 10$ and consider three scenarios ('high', 'medium' and 'low' sparsity), under which 90%, 80% and 50% of the off-diagonal elements of $\boldsymbol{\alpha}$ are set to zero, indicating no interaction between the dimension pairs. The remaining off-diagonal elements of $\boldsymbol{\alpha}$ are set to the value 0.1, and the diagonal elements to the value 0.4.

Algorithms to be compared. We compare the performances of SGLD, versions of SGEM, SGVI that use the standard approximation of Lewis and Mohler (2011), and the boundary-corrected versions of SGEM and SGVI (SGEM-c and SGVI-c). Also, as a ‘gold-standard’ that does not involve subsampling, we implemented full MCMC and its boundary-corrected version (MCMC-c). Additionally, we benchmark our methods against two frequentist computational methods for MHP: the nonparametric estimation based on EM algorithm and piecewise basis kernels (EM-BK, see Zhou et al., 2013) and the maximum likelihood estimation for multidimensional exponential Hawkes process with both excitation and inhibition effects (MLE-I, see Bonnet et al., 2023).

Parameters. For the model hyperparameters from Section 2.2, we let $a_\ell = 2, b_\ell = 4, e_{k,\ell} = 2, f_{k,\ell} = 4, r_{k,\ell} = 2, s_{k,\ell} = 0.5$ for $k, \ell = 1, \dots, K$. We simulate $K_d = 50$ datasets for $T = 1000$. For every dataset, we start all algorithms at 16 different initial points to minimize the risk of convergence to a local optimum. For the tuning hyperparameters in stochastic optimization algorithms, we consider several subsampling ratios of $\kappa = \{0.01, 0.05, 0.1, 0.2, 0.3, 0.4\}$ and let $\tau = 1, \kappa = 0.51$. For SGEM and SGVI, we let $\rho_0 = 0.02$, and for SGLD we let $\rho_0 = \frac{0.1}{T\kappa}$. We chose $\delta = 0.25$ as the threshold for boundary-corrected methods.

Performance Metrics for Model Fitting. We consider the observed data likelihood defined in (2) as a measure for model fitting. Denote by $ODL_{d,\iota}$ the observed data likelihood calculated based on dataset d and initial point ι , we define $BODL_d = \max_{1 \leq \iota \leq 16} ODL_{d,\iota}$ as the best-observed data likelihood (BODL), as a basis for evaluating model performance. Finally, in order to compare model-fitting performance under different subsampling ratios and different datasets, we propose the following relative best-observed data likelihood (RBODL):

$$RBODL_{d,\kappa_1,\kappa_2} = \frac{BODL_{d,\kappa_1}}{BODL_{d,\kappa_2}}$$

where $BODL_{d,\kappa_1}, BODL_{d,\kappa_2}$ are the best-observed data likelihoods on dataset d under subsampling ratio κ_1 and κ_2 . Additionally, we refer to κ_2 as the reference subsampling ratio for $RBODL_{d,\kappa_1,\kappa_2}$. The RBODL is fairly easy to interpret, in that $RBODL_{d,\kappa_1,\kappa_2} > 1$ indicates a superior empirical performance of subsampling ratio κ_1 compared to κ_2 and vice versa.

Performance Metrics for Estimation Accuracy. We consider performance metrics for both point and uncertainty estimations. To evaluate estimation accuracy of the model parameters, we rely on the averaged root mean integrated squared error (RMISE) for α, β , and use mean absolute error (MAE) for μ on the log scale:

$$\begin{aligned} RMISE(\alpha, \beta) &:= \frac{1}{K^2} \sum_{j=1}^K \sum_{k=1}^K \sqrt{\int_0^{+\infty} \left(\phi_{j,k}^{\text{true}}(x) - \hat{\phi}_{j,k}(x) \right)^2 dx}, \\ MAE(\mu) &:= \frac{1}{K} \sum_{j=1}^K |\log(\mu_k^{\text{true}}) - \log(\hat{\mu}_k)|. \end{aligned}$$

where $\hat{\mu}_k$ is the point estimator of μ_k (the posterior mode for the stochastic gradient EM, the posterior mean under the variational approximation for the stochastic gradient variational method, and the posterior mean of the samples after burn-in for the stochastic gradient Langevin dynamics), and $\hat{\phi}_{k,\ell}(x)$ is obtained by plugging in the point estimators for $\alpha_{k,\ell}$ and $\beta_{k,\ell}$ into the exponential decay function. The RMISE is a commonly used metric for nonparametric triggering kernel estimation for MHP models (Zhou et al., 2020) and collectively evaluates the estimation performance for all model parameters.

We also evaluate the uncertainty estimates generated by the SGVI, SGLD, SGVI-c and SGLD-c models (SGEM provides point estimators, but does not directly provide estimates of the posterior variance). To do so, we consider the interval score (IS) (Gneiting and Raftery, 2007) for 95% credible intervals, which jointly evaluates the credible interval width and its coverage rate. We also separately compute the average coverage rate (ACR), defined as the proportion of correct coverages out of $2K^2 + K$ model parameters and the average credible interval length (AIW) as references.

4.2 Simulation results

Optimal subsampling ratios. Table 1 shows the RBODLs for all methods subject to three time budgets: 1, 3 and 5 minutes. We choose $\kappa = 0.01$ as the reference subsampling ratio. The results indicate that, except for SGLD run for 5 minutes, all methods reach the highest RBODL at $\kappa = 0.05$. Given that this optimum is greater than 1, this indicates that choosing a subsampling ratio around 0.05 (rather than the baseline, 0.01) leads to optimal model-fitting performance under a time budget. For a given method under fixed running time, we observe that the RBODL tends to drop as κ increases. This is likely because larger subsamples take considerably more time to process due to the quadratic computational complexity for each iteration. We also observe such drops in RBODL tend to reduce in size as running times increase, which suggests better model convergence with more computation time. Finally, we see more dramatic drops in RBODL for SGVI compared to SGEM under the same running time, which suggests that the EM algorithms tends to converge faster than VI algorithms. This result concurs with those of Zhou et al. (2020) in the non-stochastic gradient setting.

methods	running time	0.05	0.1	0.2	0.3	0.4
SGEM	1 min	1.003 (0.003)	1.002 (0.004)	1.000 (0.003)	0.999 (0.004)	0.997 (0.004)
	3 min	1.004 (0.005)	1.003 (0.005)	1.002 (0.005)	1.001 (0.006)	1.000 (0.005)
	5 min	1.003 (0.005)	1.004 (0.006)	1.002 (0.006)	1.002 (0.006)	1.001 (0.006)
SGEM-c	1 min	1.003 (0.007)	1.002 (0.006)	1.000 (0.006)	0.999 (0.006)	0.998 (0.006)
	3 min	1.003 (0.005)	1.003 (0.006)	1.002 (0.006)	1.001 (0.006)	1.000 (0.006)
	5 min	1.003 (0.008)	1.004 (0.008)	1.003 (0.007)	1.003 (0.008)	1.001 (0.008)
SGVI	1 min	1.004 (0.001)	1.002 (0.001)	1.000 (0.001)	0.997 (0.001)	0.995 (0.001)
	3 min	1.005 (0.001)	1.004 (0.001)	1.002 (0.001)	1.001 (0.001)	0.999 (0.001)
	5 min	1.005 (0.001)	1.005 (0.001)	1.003 (0.001)	1.002 (0.001)	1.000 (0.001)
SGVI-c	1 min	1.002 (0.001)	1.000 (0.001)	0.997 (0.001)	0.995 (0.001)	0.992 (0.001)
	3 min	1.002 (<0.001)	1.002 (0.001)	1.000 (0.001)	0.998 (0.001)	0.996 (0.001)
	5 min	1.002 (<0.001)	1.002 (0.001)	1.001 (0.001)	0.999 (0.001)	0.998 (0.001)
SGLD	1 min	1.001 (<0.001)	0.996 (0.001)	0.988 (0.002)	0.98 (0.004)	0.968 (0.005)
	3 min	1.001 (<0.001)	0.998 (0.001)	0.991 (0.001)	0.986 (0.003)	0.977 (0.004)
	5 min	1.001 (<0.001)	0.999 (0.001)	0.992 (0.001)	0.987 (0.002)	0.980 (0.003)

Table 1: RBODLs for SGEM, SGVI and SGLD under running times of 1, 3 and 5 minutes for the first data generation mechanism ($K = 3$), with $\kappa = 0.01$ being the reference subsampling ratio. Average RBODL across 50 datasets is shown, with standard deviations in the brackets.

Estimation accuracy. Table 2 shows the estimation performance measures, including RMISE, MAE, IS, ACR and AIW for all seven methods, along with the two frequentist benchmark methods. Similar to the previous simulation study, we run the same algorithm on 50 datasets with 16 different initial parameter values and choose the instance associated with the highest observed data likelihood for estimation performance evaluation. We keep the same stochastic optimization hyperparameters, fixing the subsampling ratio κ at 0.05. For SGLD, SGVI, SGVI-c, SGEM and SGEM-c, we run the algorithms for 30 minutes. For MCMC and MCMC-c, we run the algorithms on the whole dataset without subsampling for 15,000 iterations, which took around 12 hours to complete. We discard the first 5,000 samples as burn-in and calculate the posterior median for estimation performance evaluation. For both optimization-based frequentist methods, we run the algorithms until they have converged under the default convergence criteria. As would be expected, the MCMC algorithms have values of RMISE, MAE and IS lower than the majority of other methods. Moreover, MCMC algorithms produce coverage rates that are very close to nominal. Among the remaining methods from Section 3, SGLD shows the best uncertainty estimation performance with the lowest IS and ACR closest to the nominal rate, while SGVI-c shows the best point estimation performance with RMISE even lower than the MCMC methods. Additionally, we observe a significant improvement in both RMISE and IS for SGVI-c compared to SGVI, indicating that incorporating a boundary correction can lead to both improved point and uncertainty estimation performance for SGVI. For the frequentist benchmark methods, MLE-I has the lowest RMISE among all nine methods in this simulation scenario, while having MAE higher than most methods. EM-BK has the worst point estimation accuracy across the board.

Sensitivity analysis for different dataset sizes. We also look at how sensitive the RBODLs are to the scale of the data we have. We run the same algorithms on two sets of 50 datasets with $T = 500$ and $T = 2000$, and the RBODLs are shown in Tables 5 and 6. For the small datasets, the median RBODLs change much less than the large datasets over different subsampling ratios. This is not surprising, as it indicates that the algorithms tend to reach convergence faster for smaller datasets than the larger ones. Additionally, the optimal subsampling ratios for smaller datasets tend to be larger, indicating that there could be a fixed amount of data needed for algorithms to attain better model-fitting results.

Sensitivity analysis for the stochastic search parameters. Next, we investigate the effect of the stochastic search parameters on our previous simulation results. To this end, we rerun our analysis for the medium-sized dataset under each of the following three sets of τ_1, τ_2 values: (1) $\tau_1 = 5, \tau_2 = 0.51$, (2) $\tau_1 = 1, \tau_2 = 1$, (3) $\tau_1 = 5, \tau_2 = 1$. The results are shown in Table 7, 8 and 9. As expected, the behavior of RBODL with respect to subsampling ratio and running time is similar to the default scenario shown in Table 1. Also, the results in Table 7 are more similar to those in Table 1 than cases in Tables 8 and 9. This is because τ_2 controls the decay rate of the stepsize parameter, which has a bigger long-term effect on ρ_r compared to the delay parameter τ_1 . We also looked at the estimation performances for all five methods under these four scenarios, with

methods	RMISE (α, β)	MAE (μ)	IS	ACR	AIW
MCMC	0.042 (0.008)	0.072 (0.036)	1.042 (0.274)	0.952 (0.046)	1.015 (0.053)
	0.042 (0.008)	0.072 (0.036)	1.056 (0.278)	0.952 (0.055)	1.015 (0.058)
SGLD	0.052 (0.019)	0.109 (0.283)	3.898 (4.739)	0.667 (0.152)	0.844 (0.172)
	0.046 (0.008)	0.103 (0.048)	6.163 (2.117)	0.333 (0.131)	0.222 (0.012)
SGVI	0.040 (0.007)	0.093 (0.044)	4.905 (1.698)	0.429 (0.139)	0.213 (0.012)
	0.100 (0.076)	0.024 (0.026)	-	-	-
SGEM	0.103 (0.065)	0.023 (0.022)	-	-	-
	0.340 (0.009)	2.065 (0.256)	-	-	-

Table 2: Estimation metrics across all nine methods for the first data generation mechanism ($K = 3$). The values in the grid cells are the average across 50 datasets, with the standard deviation in the brackets.

performance metrics shown in Table 10 and 11. We can see that all algorithms performed significantly better in scenarios where $\tau_2 = 0.51$, indicating that a large value of τ_2 may lead to suboptimal estimates because algorithms converged too fast. We also note that the SGEM-c outperformed SGEM where $\tau_2 = 0.51$.

Sensitivity analysis for the threshold values of the boundary-corrected methods. Previously, we chose a fixed value $\delta = 0.25$ as the common threshold for all boundary-corrected methods. In this simulation study, we investigate a systematic way of choosing δ based on the discussion in Section 2.1, and study the parameter estimation performance under different values of δ . Given an estimate for β and a fixed value $r > 0$, we find δ such that $\delta = \frac{1}{K^2} \sum_{j=1}^K \sum_{k=1}^K \frac{1}{\beta_{k,\ell}}$. Table 12 shows the point and uncertainty estimation results for SGVI-c and SGEM-c under values of $r \in \{0.5, 1, 2, 3, 4\}$. For both methods, all estimation metrics reached optimality between $r = 1$ and $r = 2$.

methods	RMISE (α, β)	MAE (μ)	IS	ACR	AIW
MCMC-rw	0.044 (0.008)	0.075 (0.037)	1.242 (0.418)	0.951 (0.057)	1.037 (0.063)
	0.050 (0.012)	0.113 (0.047)	2.494 (1.483)	0.763 (0.111)	0.876 (0.120)
SGLD-apx	0.050 (0.012)	0.113 (0.047)	2.494 (1.483)	0.763 (0.111)	0.876 (0.120)

Table 3: Estimation metrics for MCMC-rw and SGLD-apx for the first data generation mechanism ($K = 3$). The values in the grid cells are the average across 50 datasets, with the standard deviation in the brackets.

Sensitivity analysis for boundary approximation. To numerically show that the boundary approximations in (5) and (6) does not lead to a significant information loss, we implemented two additional methods as a comparison: the full MCMC algorithm with random-walk updates for β using the full likelihood (MCMC-rw), and the Langevin dynamics algorithm with likelihood approximation (SGLD-apx). We focus on these two algorithms here because they are ones where both the true and the various approximate likelihoods can be implemented in a straightforward fashion. Table 3 shows the results for these two methods, which should be compared with those for MCMC, MCMC-c and SGLD in Table 10. The results suggest that the errors introduced by the approximation are negligible (at least, compared to the Monte Carlo error involved), both in terms of both point and uncertainty estimation.

Robustness to model sparsity. Our last evaluation uses the alternative data generation mechanism described in Section 4.1 where we have a ten-dimensional MHP with varying degrees of sparsity in α . Table 4 shows the average and standard deviation of the estimation metrics for all five methods and the two frequentist benchmarks. Due to presence of sparsity, the metrics for the $\alpha_{k,\ell}$ s and $\beta_{k,\ell}$ s are evaluated only for entries that are associated with a non-zero true value for $\alpha_{k,\ell}$. Note that, unlike the first simulation scenario, MLE-I and EM-BK perform significantly worse than the Bayesian methods in all of our simulations with $K = 10$. Furthermore, MLE-I takes much longer time to converge compared to the three-dimensional scenario. For example, the average running time for the ‘low sparsity’ scenario is 61.47 minutes, which is much longer than the 30-minute running time for all five stochastic Bayesian methods. Aside from this, the results are largely consistent those from the original, three-dimensional data generation mechanism. SGVI and SGVI-c have the best point estimation performance, SGEM and SGEM-c have the worst, and SGLD is in between. Furthermore, scenarios that are less sparse tend to be associated with lower estimation errors.

5 Real-world application

Data description. In this section, we apply our methods to model the market risk dynamics in the Standard & Poor (S&P)’s 500 intraday index prices for its 11 sectors: Consumer Discretionary (COND), Communication Staples (CONS), Energy (ENRS), Financials (FINL), Health Care (HLTH), Industrials (INDU), Information Technology (INFT), Materials (MATR), Real Estate (RLST), Communication Services (TELS), Utilities (UTIL). To achieve this, price data between August 22, 2022 and Jan 23, 2023 was downloaded from Bloomberg Finance L.P. Similar to Rodríguez et al. (2017), an event occurs on dimension $k = 1, \dots, 11$ if the negative log returns in sector k exceeds a predetermined threshold (in our case, a 0.05% drop on a one-minute basis). The resulting dataset contains 55,509 events across the 11 dimensions.

Results. We fit a Hawkes process model with exponential decay functions to the event data using the SGEM, SGEM-c, SGVI, SGVI-c and SGLD algorithms. We set the subsampling ratio of $\kappa = 0.01$ for SGLD and of $\kappa = 0.05$ for all other methods. Similar to the procedure in Section 4.1, we start all algorithms at 16 different initial points and choose the instances with the highest observed data likelihood to compute the estimates. Furthermore, all these algorithms were run for a fixed period of 30 minutes for each initial set of values. As a reference, we also apply MCMC and MCMC-c to the dataset and use 10,000 posterior samples after 10,000 burn-ins, which roughly took around two days.

Figure 2 shows heatmaps of point estimates for the α parameters for all seven algorithms. To facilitate comparisons, we also generate a visual representation by constructing a measure of similarity between sectors i and j as $\Upsilon(i, j) = \exp\left\{-\frac{1}{2}(\alpha_{ij} + \alpha_{ji})\right\}$, and then use multidimensional scaling (Torgerson, 1952) to find a two-dimensional representation of these similarities. Because the representation is arbitrary up to translations, rotations and reflections, we use Procrustes analysis (Dryden and Mardia, 2016) to align the representations for all the algorithms. All seven methods yield similar point estimates for α . To explore this question in more detail, we present in Table 13 the mean square distance between point estimates for each pair of methods. We see that MCMC and MCMC-c are almost identical, and that SGEM, SGVI, and SGEM-c yield very similar estimates. Interestingly, SGVI-c yields results that are as close to those of the MCMC “gold standard” as those from SGEM, SGVI, and SGEM-c, but that are fairly different from them. We also note that SGLD seems to yield results that are the furthest away from the MCMC procedures, suggesting that a time budget of 30 minutes is not enough to achieve reliable results in this example. From a substantive point of view, Figure 2 suggests mutual excitation of exceedances within each of the following three groups: (1) UTIL, MATR, COND, (2) INFT, FINL and INDU, (3) TELS, RLST, HLTH and CONS and ENRS. One particular interesting result is the estimates for the energy (ENRS) sector, which has a much higher diagonal α estimate and lower off diagonal estimates corresponding to other sectors. This is supported by the scatterplot of principal coordinates, in which the point for ENRS is away from all other sectors, indicating that such sector may be less likely associated with price movements in other sectors.

Next, we show in Figure 3 point estimates of β under all 7 methods and, in Table 14, the mean square distance between the estimates generated by the different methods. The pattern of the results is very similar: (1) MCMC and MCMC-c yield the most similar results, (2) SGLD seems to yield estimates that are furthest away from those generated by the MCMC methods, (3) SGEM, SGVI, and SGEM-c yield very similar results to each other, and (4) SGVI-c yields different results from SGEM, SGVI, and SGEM-c, but they are as close to those of the MCMC approaches as those from the three alternatives. We note, however, that the estimates of β generated by MCMC and MCMC-c do seem to differ from each other much more than than the estimates of α did.

Figure 4 shows the point estimates for μ , and Table 15 shows mean square distances between the model estimates. Not surprisingly, the same patterns arise again, although we note that the distances tend to be smaller. From an application point of view, we note that all methods identify ENRS as a sector with a very high baseline rate events, FINL, INFT, INDU, HLTH and CONS as sectors where the majority of price drops are the result of contagion from turbulence in other sectors.

As for uncertainty estimation, Figures 5, 6 and 7 show the length of the estimated posterior credible intervals for α , β and μ for SGVI, SGVI-c and SGLD, as well as for MCMC and MCMC-c. As was the case with simulated datasets, stochastic

methods	sparsity	RMISE (α, β)	MAE (μ)	IS	ACR	AIW
SGLD	high	0.048 (0.005)	0.295 (0.035)	1.562 (0.546)	0.742 (0.033)	1.003 (0.085)
	medium	0.041 (0.005)	0.256 (0.037)	2.172 (0.680)	0.802 (0.036)	1.327 (0.144)
	low	0.031 (0.003)	0.171 (0.018)	2.915 (1.033)	0.841 (0.034)	1.443 (0.072)
SGVI	high	0.047 (0.013)	0.179 (0.038)	2.011 (0.735)	0.699 (0.059)	0.680 (0.112)
	medium	0.040 (0.008)	0.158 (0.039)	3.158 (1.131)	0.704 (0.053)	0.766 (0.105)
	low	0.030 (0.004)	0.111 (0.029)	5.264 (1.269)	0.620 (0.045)	0.664 (0.089)
SGVI-c	high	0.047 (0.012)	0.183 (0.038)	1.904 (0.729)	0.703 (0.062)	0.665 (0.047)
	medium	0.039 (0.008)	0.163 (0.039)	2.941 (1.051)	0.710 (0.055)	0.747 (0.051)
	low	0.029 (0.004)	0.118 (0.029)	4.515 (1.110)	0.637 (0.048)	0.638 (0.033)
SGEM	high	0.047 (0.007)	0.308 (0.033)	-	-	-
	medium	0.039 (0.005)	0.263 (0.030)	-	-	-
	low	0.030 (0.003)	0.160 (0.026)	-	-	-
SGEM-c	high	0.047 (0.006)	0.263 (0.034)	-	-	-
	medium	0.039 (0.005)	0.161 (0.030)	-	-	-
	low	0.030 (0.003)	0.161 (0.027)	-	-	-
MLE-I	high	0.206 (0.015)	0.331 (0.151)	-	-	-
	medium	0.155 (0.008)	0.421 (0.199)	-	-	-
	low	0.124 (0.003)	0.247 (0.195)	-	-	-
EM-BK	high	0.462 (0.047)	0.584 (0.106)	-	-	-
	medium	0.366 (0.048)	0.445 (0.106)	-	-	-
	low	0.261 (0.019)	0.197 (0.088)	-	-	-

Table 4: Estimation metrics across SGLD, SGVI, SGVI-c, SGEM , SGEM-c, MLE-I and EM-BK for the second data generation mechanism ($K = 10$) with three levels of model sparsity. The values in the grid cells are the average across 50 datasets, with the standard deviation in the brackets.

gradient methods seem to underestimate the uncertainty in the posterior distribution, with SGVI and SGVI-c doing much more dramatically than SGLD.

Finally, we conduct in-sample goodness-of-fit analysis using quantile-quantile plots for the posterior distribution of inter-event times. The construction of these plots relies on the well-known time-rescaling theorem (Daley and Vere-Jones, 2008), which states that, if the Hawkes model process is correct, the transformed inter-arrival times on dimension ℓ , $z_i^\ell = 1 - \exp\{-[\Lambda_\ell(t_i^\ell) - \Lambda_\ell(t_{i-1}^\ell)]\}$, where $\Lambda_\ell(t) = \int_0^t \lambda_\ell(s)ds$ is the compensator for $\lambda_\ell(t)$), follow a uniform distribution on the unit interval. Quantile-quantile plots of the (transformed) observed inter-arrival vs. those for the uniform distribution for all seven methods are shown in the Supplementary Materials. All seven methods produce very similar results. In all cases, the plots suggests that a MHP model tends to predict somewhat shorter inter-arrival times than expected.

6 Discussion

Our experiments indicate that computational methods for Hawkes process models based on stochastic gradients can lead to accurate estimators and substantially reduce the computational burden in large datasets. However, our results also indicate some clear tradeoffs. SGEM algorithms are the fastest (which is consistent with the results of Zhou et al. (2020) for full-batch methods), but they do not yield interval estimates of the parameters. SGVI algorithms are almost as computationally efficient as SGEM and yield interval estimates. However, these interval estimates are too narrow, leading to substantial undercoverage. That variational inference underestimates the variance of the posterior distribution is well known (e.g., see Blei et al., 2017), but it was still striking to see how low the coverage can be in the case of MHPs. SGLD algorithms are the slowest and require careful tuning, but can also lead to more accurate interval estimates if allowed to run for enough time.

Our experiments also suggest that the new approximation to the full-data likelihood based on a first-order Taylor expansion of the compensator of the Hawkes process has the potential to improve the accuracy of the algorithm with minimal additional computational costs. This was clearer for SGVI algorithms, where the approximation clearly improved the MSE of the point estimators. Finally, our experiments suggest that, as sample sizes grow, the fraction of time involved in the subsamples used to compute stochastic gradients can decrease as long as the number of observations in each subsample remains above a critical threshold. This is important, because it suggests that, at least empirically, the computational complexity of this algorithms can remain roughly constant as a function of the sample size.

As pointed out by one of the referees, an often important question in the context of MHPs is to identify which interactions are non-null. Bayesian inference for the the interaction graph can be accommodated through a slight modification of the priors in Section 2.2 in which the single Gamma prior for $\alpha_{k,\ell}$ is replaced by a “spike-and-slab” style specification (e.g., see Mitchell and Beauchamp, 1988) which, in this case, can be defined through a mixture of two Gamma priors with very different means. Extending our algorithms to this setting is straightforward, perhaps requiring the introduction of additional latent component indicators for each of the $\alpha_{k,\ell}$ s. Our numerical explorations of this variant of the model suggest that the SGEM and SGVI algorithms perform quite well in this setting, but the SGLD algorithm struggles to properly explore the parameter space. Another important question is how these methods extend to non-linear Hawkes processes (e.g., see Brémaud and Massoulié, 1996), which allows for the $\alpha_{k,\ell}$ s to take negative values. With the addition of a nonlinear activation layer in the intensity function, nonlinear MHP models break model conjugacy and therefore cause computational challenges for SGEM and SGVI. For certain non-linear MHP models, latent variable augmentation can be used to restore model conjugacy, enabling a more or less direct extension of the algorithms described here (e.g., see Malem-Shinitski et al., 2021; Zhou et al., 2021). Alternatives that could be used in more general settings include methods based on Laplace approximations (e.g., see (Wang and Blei, 2013)) and non-conjugate message passing (e.g., see Khan and Lin, 2017), which have been successfully applied in other model settings. However, as far we are aware, these have not yet been explored for general non-linear Hawkes process. On the other hand, since SGLD does not rely on conjugacy, its extension to nonlinear MHP is relatively more straightforward than SGEM and SGVI.

The work in this manuscript focused on a very particular class of MHP with constant baseline intensity and a parametric excitation function. This was a deliberate choice meant to simplify exposition and interpretation. However, the insights from this manuscript apply much more broadly. For example, we are currently work on fast inference algorithms for MHP models where the excitation functions are modeled non parametrically using mixtures of dependent Dirichlet processes. This, and other extensions, will be discussed elsewhere.

Reproducibility information

The R scripts for the algorithms were run on CentOS 7 Linux, with 128GB of memory. The dataset and the R code for the simulation and application examples can be found at <https://github.com/AlexJiang1125/MHP>.

Acknowledgements

This research was partially supported by NSF grants NSF-2023495 and NSF-2114727. We would also like to acknowledge the support of the Research Computing Club at the University of Washington by providing access to their computational resources. We also express our gratitude to two referees, whose feedback during the review process helped improve the manuscript.

A Loss of information from the boundary-corrected likelihood approximation

Given the time domain $(0, T]$ and approximation threshold δ , We define $\varphi_{k,\ell}(\delta, T)$ as the **information loss ratio** for approximating $\Lambda_{k,\ell}(\cdot)$, which has the following formula:

$$\varphi_{k,\ell}(\delta, T) = \frac{1}{T} \int_0^T \left[1 - \frac{1 - \exp(-\beta_{k,\ell}(T-t))}{\mathbf{1}(0 < t \leq T - \delta) + [\beta_{k,\ell}(T-t)] \cdot \mathbf{1}(T - \delta < t \leq T)} \right] dt. \quad (16)$$

We can interpret $\varphi_{k,\ell}(\delta, T)$ as follows: suppose t is a time event on dimension k , $\varphi_{k,\ell}(\delta, T)$ is one minus the ratio of t 's contribution to the compensator (sans the common term $\mu_k T$), integrated over a uniform distribution for t on $[0, T]$. The use of a uniform distribution here seems appropriate under the assumption that the MHP is stationary.

Theorem 1. *Assuming $\max_{k,\ell} |\beta_{k,\ell}| \leq M$ and δ is fixed, the information loss ratio converges to zero as $T \rightarrow \infty$, i.e.*

$$\lim_{T \rightarrow \infty} \max_{1 \leq k, \ell \leq K} |\varphi_{k,\ell}(\delta, T)| = 0.$$

Proof. We proved the theorem by showing that $\lim_{T \rightarrow \infty} |\varphi_{k,\ell}(\delta, T)| = 0$ for all $k, \ell = 1, \dots, K$. To derive an upper bound on $|\varphi_{k,\ell}(\delta, T)|$, we start by breaking down the integration domain into two parts: $(0, T - \delta]$ and $(T - \delta, T]$. For the first part, we have:

$$\left| \frac{1}{T} \int_0^{T-\delta} [1 - (1 - \exp(-\beta_{k,\ell}(T-t)))] dt \right| = \left| \frac{1}{T} \int_0^{T-\delta} \exp(-\beta_{k,\ell} t) dt \right| = \frac{1}{\beta_{k,\ell} T} [1 - \exp(-\beta_{k,\ell}(T - \delta))].$$

For the second part, we have:

$$\begin{aligned} \left| \frac{1}{T} \int_{T-\delta}^T \left[1 - \frac{1 - \exp(-\beta_{k,\ell}(T-t))}{[\beta_{k,\ell}(T-t)]} \right] dt \right| &= \frac{1}{\beta_{k,\ell} T} \int_0^{\beta_{k,\ell} \delta} \frac{s - 1 - \exp(-s)}{s} ds \\ &= \frac{1}{\beta_{k,\ell} T} \int_0^{\beta_{k,\ell} \delta} \frac{\exp(-2\Delta s) s^2}{2s} ds, \quad (0 \leq \Delta s \leq s) \\ &\leq \frac{1}{\beta_{k,\ell} T} \int_0^{\beta_{k,\ell} \delta} \frac{s}{2} ds = \frac{\beta_{k,\ell} \delta^2}{4T}. \end{aligned}$$

Assuming δ is fixed and $\beta_{k,\ell}$ is bounded by a fixed constant over $k, \ell = 1, \dots, K$, both parts converge to zero as $T \rightarrow \infty$. As $|\varphi_{k,\ell}(\delta, T)|$ is upper bounded by the two parts above, we showed that $\lim_{T \rightarrow \infty} |\varphi_{k,\ell}(\delta, T)| = 0$. \square

References

Bacry, E., Bompaire, M., Gaiffas, S., and Muzy, J.-F. (2020). Sparse and low-rank multivariate hawkes processes. *Journal of Machine Learning Research*, 21(50):1–32.

Bacry, E., Mastromatteo, I., and Muzy, J.-F. (2015). Hawkes processes in finance. *Market Microstructure and Liquidity*, 1(01):1550005.

Bishop, C. M. and Nasrabadi, N. M. (2006). *Pattern recognition and machine learning*. Springer.

Blei, D. M. and Jordan, M. I. (2006). Variational inference for Dirichlet process mixtures. *Bayesian Analysis*, 1(1):121 – 143.

Blei, D. M., Kucukelbir, A., and McAuliffe, J. D. (2017). Variational inference: A review for statisticians. *Journal of the American statistical Association*, 112(518):859–877.

Bonnet, A., Martinez Herrera, M., and Sangnier, M. (2023). Inference of multivariate exponential hawkes processes with inhibition and application to neuronal activity. *Statistics and Computing*, 33(4):91.

Bottou, L. and Bousquet, O. (2007). The tradeoffs of large scale learning. In Platt, J., Koller, D., Singer, Y., and Roweis, S., editors, *Advances in Neural Information Processing Systems*, volume 20. Curran Associates, Inc.

Brémaud, P. and Massoulié, L. (1996). Stability of nonlinear hawkes processes. *The Annals of Probability*, pages 1563–1588.

Cappe, O. and Moulines, E. (2009). On-line expectation maximization algorithm for latent data models. *Journal of the Royal Statistical Society: Series B (Statistical Methodology)*, 71(3):593–613.

Chen, J., Zhu, J., Teh, Y. W., and Zhang, T. (2018). Stochastic expectation maximization with variance reduction. *Advances in Neural Information Processing Systems*, 31.

Chen, T., Fox, E., and Guestrin, C. (2014). Stochastic gradient Hamiltonian Monte Carlo. In *International conference on machine learning*, pages 1683–1691. PMLR.

Daley, D. J. and Vere-Jones, D. (2008). *An Introduction to the Theory of Point Processes. Volume II: General Theory and Structure*. Springer.

Dempster, A. P., Laird, N. M., and Rubin, D. B. (1977). Maximum likelihood from incomplete data via the EM algorithm. *Journal of the Royal Statistical Society: Series B (Methodological)*, 39(1):1–22.

Deutsch, I. and Ross, G. J. (2022). Bayesian estimation of multivariate hawkes processes with inhibition and sparsity. *arXiv preprint arXiv:2201.05009*.

Donnet, S., Rivoirard, V., and Rousseau, J. (2020). Nonparametric Bayesian estimation for multivariate Hawkes processes. *Annals of Statistics*, 48:2698–2727.

Dryden, I. L. and Mardia, K. V. (2016). *Statistical shape analysis: with applications in R*, volume 995. John Wiley & Sons.

Foti, N., Xu, J., Laird, D., and Fox, E. (2014). Stochastic variational inference for hidden Markov models. *Advances in neural information processing systems*, 27.

Gneiting, T. and Raftery, A. E. (2007). Strictly proper scoring rules, prediction, and estimation. *Journal of the American Statistical Association*, 102(477):359–378.

Gopalan, P. K., Gerrish, S., Freedman, M., Blei, D., and Mimno, D. (2012). Scalable inference of overlapping communities. *Advances in Neural Information Processing Systems*, 25.

Hawkes, A. G. (1971). Spectra of some self-exciting and mutually exciting point processes. *Biometrika*, 58(1):83–90.

Hawkes, A. G. and Oakes, D. (1974). A cluster process representation of a self-exciting process. *Journal of Applied Probability*, 11(3):493–503.

Hoffman, M. D., Blei, D. M., Wang, C., and Paisley, J. (2013). Stochastic variational inference. *J. Mach. Learn. Res.*, 14(1):1303–1347.

Holbrook, A. J., Ji, X., and Suchard, M. A. (2022). From viral evolution to spatial contagion: a biologically modulated Hawkes model. *Bioinformatics*, 38(7):1846–1856.

Holbrook, A. J., Loeffler, C. E., Flaxman, S. R., and Suchard, M. A. (2021). Scalable Bayesian inference for self-excitatory stochastic processes applied to big american gunfire data. *Statistics and computing*, 31(1):1–15.

Khan, M. and Lin, W. (2017). Conjugate-computation variational inference: Converting variational inference in non-conjugate models to inferences in conjugate models. In *Artificial Intelligence and Statistics*, pages 878–887. PMLR.

Lewis, E. and Mohler, G. (2011). A nonparametric EM algorithm for multiscale Hawkes processes. *Journal of Nonparametric Statistics*.

Linderman, S. W. and Adams, R. P. (2015). Scalable Bayesian inference for excitatory point process networks. *arXiv preprint arXiv:1507.03228*.

Linderman, S. W., Wang, Y., and Blei, D. M. (2017). Bayesian inference for latent hawkes processes. *Advances in Neural Information Processing Systems*.

Liniger, T. J. (2009). *Multivariate Hawkes processes*. PhD thesis, ETH Zurich.

Logothetis, A. and Krishnamurthy, V. (1999). Expectation maximization algorithms for MAP estimation of jump Markov linear systems. *IEEE Transactions on Signal Processing*, 47(8):2139–2156.

Malem-Shinitzki, N., Ojeda, C., and Opper, M. (2021). Nonlinear hawkes process with gaussian process self effects. *arXiv preprint arXiv:2105.09618*.

Malem-Shinitzki, N., Ojeda, C., and Opper, M. (2022). Variational bayesian inference for nonlinear hawkes process with gaussian process self-effects. *Entropy*, 24(3):356.

Marsan, D. and Lengline, O. (2008). Extending earthquakes' reach through cascading. *Science*, 319(5866):1076–1079.

Mei, H. and Eisner, J. M. (2017). The neural Hawkes process: A neurally self-modulating multivariate point process. In Guyon, I., Luxburg, U. V., Bengio, S., Wallach, H., Fergus, R., Vishwanathan, S., and Garnett, R., editors, *Advances in Neural Information Processing Systems*, volume 30. Curran Associates, Inc.

Mitchell, T. J. and Beauchamp, J. J. (1988). Bayesian variable selection in linear regression. *Journal of the american statistical association*, pages 1023–1032.

Mohler, G. (2013). Modeling and estimation of multi-source clustering in crime and security data. *The Annals of Applied Statistics*, pages 1525–1539.

Neal, R. (2011). MCMC Using Hamiltonian Dynamics. In *Handbook of Markov Chain Monte Carlo*, pages 113–162. CRC Press.

Nemeth, C. and Fearnhead, P. (2021). Stochastic gradient Markov chain Monte Carlo. *Journal of the American Statistical Association*, 116(533):433–450.

Nickel, M. and Le, M. (2020). Learning multivariate hawkes processes at scale. *arXiv preprint arXiv:2002.12501*.

Ogata, Y. (1988). Statistical models for earthquake occurrences and residual analysis for point processes. *Journal of the American Statistical association*, 83(401):9–27.

Ozaki, T. (1979). Maximum likelihood estimation of Hawkes' self-exciting point processes. *Annals of the Institute of Statistical Mathematics*, 31:145–155.

Rasmussen, J. G. (2013). Bayesian inference for Hawkes processes. *Methodology and Computing in Applied Probability*, 15(3):623–642.

Rizoiu, M.-A., Lee, Y., Mishra, S., and Xie, L. (2017). Hawkes processes for events in social media. In Chang, S.-F., editor, *Frontiers of multimedia research*, pages 191–218. Morgan & Claypool Publishers.

Robbins, H. and Monro, S. (1951). A Stochastic Approximation Method. *The Annals of Mathematical Statistics*, 22(3):400 – 407.

Rodríguez, A., Wang, Z., and Kottas, A. (2017). Assessing systematic risk in the S&P500 index between 2000 and 2011: A Bayesian nonparametric approach. *The Annals of Applied Statistics*, pages 527–552.

Schoenberg, F. P. (2013). Facilitated estimation of etas. *Bulletin of the seismological Society of America*, 103(1):601–605.

Sulem, D., Rivoirard, V., and Rousseau, J. (2021). Bayesian estimation of nonlinear hawkes process. *arXiv preprint arXiv:2103.17164*.

Sulem, D., Rivoirard, V., and Rousseau, J. (2022). Scalable variational bayes methods for hawkes processes. *arXiv preprint arXiv:2212.00293*.

Torgerson, W. S. (1952). Multidimensional scaling: I. theory and method. *Psychometrika*, 17(4):401–419.

Veen, A. and Schoenberg, F. P. (2008). Estimation of space–time branching process models in seismology using an em–type algorithm. *Journal of the American Statistical Association*, 103(482):614–624.

Wainwright, M. J., Jordan, M. I., et al. (2008). Graphical models, exponential families, and variational inference. *Foundations and Trends® in Machine Learning*, 1(1–2):1–305.

Wang, C. and Blei, D. M. (2013). Variational inference in nonconjugate models. *Journal of Machine Learning Research*.

Welling, M. and Teh, Y. W. (2011). Bayesian learning via stochastic gradient langevin dynamics. In *Proceedings of the 28th international conference on machine learning (ICML-11)*, pages 681–688.

Xu, H. and Zha, H. (2017). A Dirichlet mixture model of hawkes processes for event sequence clustering. *Advances in neural information processing systems*, 30.

Zhang, R., Walder, C., Rizoiu, M.-A., and Xie, L. (2018). Efficient non-parametric Bayesian Hawkes processes. *arXiv preprint arXiv:1810.03730*.

Zhou, F., Kong, Q., Zhang, Y., Feng, C., and Zhu, J. (2021). Nonlinear hawkes processes in time-varying system. *arXiv preprint arXiv:2106.04844*.

Zhou, F., Li, Z., Fan, X., Wang, Y., Sowmya, A., and Chen, F. (2020). Efficient inference for nonparametric Hawkes processes using auxiliary latent variables. *Journal of Machine Learning Research*.

Zhou, K., Zha, H., and Song, L. (2013). Learning triggering kernels for multi-dimensional Hawkes processes. In *International conference on machine learning*, pages 1301–1309. PMLR.

methods	running time	0.05	0.1	0.2	0.3	0.4
SGEM	1 min	0.999 (0.002)	0.998 (0.002)	0.994 (0.002)	0.993 (0.002)	0.991 (0.003)
	3 min	1.001 (0.003)	0.999 (0.003)	0.997 (0.003)	0.996 (0.003)	0.994 (0.003)
	5 min	1.001 (0.009)	1.000 (0.008)	0.999 (0.008)	0.997 (0.009)	0.996 (0.009)
SGEM-c	1 min	1.003 (0.010)	0.998 (0.017)	0.996 (0.022)	1.000 (0.025)	1.000 (0.027)
	3 min	1.006 (0.006)	1.003 (0.01)	0.994 (0.018)	0.994 (0.021)	0.998 (0.023)
	5 min	1.007 (0.007)	1.006 (0.009)	1.003 (0.015)	1.002 (0.02)	1.003 (0.023)
SGVI	1 min	0.999 (< 0.001)	0.996 (0.001)	0.991 (0.001)	0.988 (0.001)	0.986 (0.002)
	3 min	1.001 (< 0.001)	0.999 (< 0.001)	0.995 (0.001)	0.992 (0.001)	0.99 (0.001)
	5 min	1.001 (< 0.001)	1.000 (< 0.001)	0.997 (< 0.001)	0.994 (0.001)	0.992 (0.001)
SGVI-c	1 min	0.998 (< 0.001)	0.995 (0.001)	0.991 (0.001)	0.988 (0.001)	0.985 (0.002)
	3 min	1.000 (< 0.001)	0.998 (< 0.001)	0.994 (0.001)	0.992 (0.001)	0.99 (0.001)
	5 min	1.000 (< 0.001)	0.999 (< 0.001)	0.996 (0.001)	0.993 (0.001)	0.991 (0.001)
SGLD	1 min	0.997 (0.001)	0.991 (0.002)	0.98 (0.003)	0.96 (0.005)	0.945 (0.010)
	3 min	0.999 (0.001)	0.993 (0.001)	0.985 (0.002)	0.973 (0.003)	0.959 (0.005)
	5 min	0.999 (0.001)	0.993 (0.001)	0.985 (0.002)	0.973 (0.003)	0.959 (0.005)

Table 5: Sensitivity analysis for the dataset sizes, with a large dataset ($T = 2000$) for the first data generation mechanism ($K = 3$). RBODLs for SGEM, SGVI and SGLD under running times of 1, 3 and 5 minutes, with $\kappa = 0.01$ being the reference subsampling ratio. Average RBODL across 50 datasets is shown, with standard deviations in the brackets.

methods	running time	0.05	0.1	0.2	0.3	0.4
SGEM	1 min	1.008 (0.008)	1.008 (0.005)	1.008 (0.005)	1.007 (0.005)	1.006 (0.005)
	3 min	1.007 (0.007)	1.008 (0.006)	1.008 (0.007)	1.007 (0.006)	1.007 (0.007)
	5 min	1.008 (0.01)	1.008 (0.009)	1.009 (0.009)	1.008 (0.009)	1.008 (0.009)
SGEM-c	1 min	1.003 (0.012)	1.003 (0.012)	1.002 (0.011)	1.001 (0.011)	1.001 (0.011)
	3 min	1.003 (0.007)	1.003 (0.007)	1.004 (0.007)	1.003 (0.007)	1.003 (0.007)
	5 min	1.002 (0.006)	1.003 (0.006)	1.003 (0.005)	1.002 (0.006)	1.002 (0.006)
SGVI	1 min	1.032 (0.009)	1.032 (0.009)	1.03 (0.009)	1.029 (0.009)	1.027 (0.009)
	3 min	1.032 (0.009)	1.032 (0.009)	1.032 (0.009)	1.031 (0.009)	1.03 (0.009)
	5 min	1.033 (0.009)	1.033 (0.009)	1.033 (0.009)	1.032 (0.009)	1.032 (0.009)
SGVI-c	1 min	1.021 (0.007)	1.021 (0.007)	1.019 (0.007)	1.018 (0.007)	1.016 (0.007)
	3 min	1.022 (0.007)	1.022 (0.007)	1.022 (0.007)	1.021 (0.007)	1.02 (0.007)
	5 min	1.022 (0.007)	1.022 (0.007)	1.022 (0.007)	1.022 (0.007)	1.021 (0.007)
SGLD	1 min	1.017 (0.006)	1.015 (0.006)	1.008 (0.005)	1.004 (0.005)	0.997 (0.004)
	3 min	1.019 (0.006)	1.018 (0.006)	1.014 (0.006)	1.009 (0.005)	1.005 (0.005)
	5 min	1.020 (0.006)	1.020 (0.006)	1.017 (0.006)	1.011 (0.005)	1.007 (0.005)

Table 6: Sensitivity analysis for the dataset sizes, with a large dataset ($T = 500$) for the first data generation mechanism ($K = 3$). RBODLs for SGEM, SGVI and SGLD under running times of 1, 3 and 5 minutes, with $\kappa = 0.01$ being the reference subsampling ratio. Average RBODL across 50 datasets is shown, with standard deviations in the brackets.

methods	running time	0.05	0.1	0.2	0.3	0.4
SGEM	1 min	1.003 (0.007)	1.002 (0.005)	1.000 (0.005)	0.997 (0.005)	0.995 (0.005)
	3 min	1.004 (0.006)	1.003 (0.005)	1.002 (0.006)	1.000 (0.006)	0.998 (0.006)
	5 min	1.003 (0.008)	1.004 (0.008)	1.003 (0.008)	1.001 (0.008)	1.000 (0.008)
SGEM-c	1 min	1.003 (0.005)	1.003 (0.005)	1.000 (0.004)	0.998 (0.004)	0.996 (0.005)
	3 min	1.003 (0.009)	1.004 (0.008)	1.003 (0.008)	1.001 (0.008)	1.001 (0.008)
	5 min	1.004 (0.006)	1.003 (0.006)	1.003 (0.006)	1.002 (0.006)	1.001 (0.006)
SGVI	1 min	1.003 (0.005)	1.001 (0.005)	0.998 (0.005)	0.996 (0.005)	0.993 (0.005)
	3 min	1.003 (0.006)	1.004 (0.006)	1.002 (0.006)	1.000 (0.007)	0.998 (0.006)
	5 min	1.004 (0.006)	1.004 (0.006)	1.003 (0.006)	1.001 (0.006)	1.000 (0.006)
SGVI-c	1 min	1.003 (0.003)	1.003 (0.002)	1.000 (0.002)	0.998 (0.002)	0.996 (0.002)
	3 min	1.004 (0.006)	1.004 (0.005)	1.003 (0.005)	1.002 (0.005)	1.000 (0.005)
	5 min	1.003 (0.012)	1.003 (0.012)	1.003 (0.012)	1.002 (0.012)	1.001 (0.012)
SGLD	1 min	1.004 (0.001)	1.001 (0.001)	0.996 (0.001)	0.993 (0.001)	0.99 (0.002)
	3 min	1.003 (0.001)	1.003 (0.001)	1.000 (0.001)	0.997 (0.001)	0.995 (0.001)
	5 min	1.003 (0.001)	1.003 (0.001)	1.001 (0.001)	0.999 (0.001)	0.997 (0.001)

Table 7: Sensitivity analysis for the stochastic search parameters for the first data generation mechanism ($K = 3$), with $\tau_1 = 5, \tau_2 = 0.51$. RBODLs for SGEM, SGVI and SGLD under running times of 1, 3 and 5 minutes, with $\kappa = 0.01$ being the reference subsampling ratio. Average RBODL across 50 datasets is shown, with standard deviations in the brackets.

methods	running time	0.05	0.1	0.2	0.3	0.4
SGEM	1 min	1.003 (0.007)	1.002 (0.005)	1.000 (0.005)	0.997 (0.005)	0.995 (0.005)
	3 min	1.004 (0.006)	1.003 (0.005)	1.002 (0.006)	1.000 (0.006)	0.998 (0.006)
	5 min	1.003 (0.008)	1.004 (0.008)	1.003 (0.008)	1.001 (0.008)	1.000 (0.008)
SGEM-c	1 min	1.003 (0.005)	1.003 (0.005)	1.000 (0.004)	0.998 (0.004)	0.996 (0.005)
	3 min	1.003 (0.009)	1.004 (0.008)	1.003 (0.008)	1.001 (0.008)	1.001 (0.008)
	5 min	1.004 (0.006)	1.003 (0.006)	1.003 (0.006)	1.002 (0.006)	1.001 (0.006)
SGVI	1 min	1.003 (0.005)	1.001 (0.005)	0.998 (0.005)	0.996 (0.005)	0.993 (0.005)
	3 min	1.003 (0.006)	1.004 (0.006)	1.002 (0.006)	1.000 (0.007)	0.998 (0.006)
	5 min	1.004 (0.006)	1.004 (0.006)	1.003 (0.006)	1.001 (0.006)	1.000 (0.006)
SGVI-c	1 min	1.003 (0.003)	1.003 (0.002)	1.000 (0.002)	0.998 (0.002)	0.996 (0.002)
	3 min	1.004 (0.006)	1.004 (0.005)	1.003 (0.005)	1.002 (0.005)	1.000 (0.005)
	5 min	1.003 (0.012)	1.003 (0.012)	1.003 (0.012)	1.002 (0.012)	1.001 (0.012)
SGLD	1 min	1.004 (0.001)	1.001 (0.001)	0.996 (0.001)	0.993 (0.001)	0.990 (0.002)
	3 min	1.003 (0.001)	1.003 (0.001)	1.000 (0.001)	0.997 (0.001)	0.995 (0.001)
	5 min	1.003 (0.001)	1.003 (0.001)	1.001 (0.001)	0.999 (0.001)	0.997 (0.001)

Table 8: Sensitivity analysis for the stochastic search parameters for the first data generation mechanism ($K = 3$), with $\tau_1 = 1, \tau_2 = 1$. RBODLs for SGEM, SGVI and SGLD under running times of 1, 3 and 5 minutes, with $\kappa = 0.01$ being the reference subsampling ratio. Average RBODL across 50 datasets is shown, with standard deviations in the brackets.

methods	running time	0.05	0.1	0.2	0.3	0.4
SGEM	1 min	1.000 (0.006)	0.999 (0.006)	0.997 (0.007)	0.997 (0.006)	0.995 (0.006)
	3 min	0.999 (0.009)	1.000 (0.009)	0.997 (0.009)	0.997 (0.009)	0.997 (0.009)
	5 min	1.000 (0.007)	0.998 (0.006)	0.998 (0.007)	0.997 (0.007)	0.996 (0.007)
SGEM-c	1 min	1.000 (0.009)	1.000 (0.010)	1.000 (0.01)	0.999 (0.011)	0.999 (0.011)
	3 min	1.000 (0.005)	1.000 (0.004)	0.999 (0.005)	0.999 (0.005)	0.998 (0.006)
	5 min	1.001 (0.009)	1.000 (0.009)	1.000 (0.009)	0.999 (0.009)	0.998 (0.009)
SGVI	1 min	0.998 (0.002)	0.995 (0.003)	0.991 (0.004)	0.989 (0.005)	0.987 (0.006)
	3 min	0.998 (0.002)	0.996 (0.003)	0.993 (0.004)	0.992 (0.004)	0.990 (0.004)
	5 min	0.999 (0.002)	0.997 (0.003)	0.995 (0.003)	0.993 (0.004)	0.991 (0.004)
SGVI-c	1 min	0.996 (0.002)	0.993 (0.003)	0.990 (0.004)	0.988 (0.005)	0.985 (0.006)
	3 min	0.997 (0.002)	0.994 (0.003)	0.992 (0.004)	0.990 (0.004)	0.989 (0.005)
	5 min	0.997 (0.002)	0.995 (0.003)	0.992 (0.003)	0.991 (0.004)	0.990 (0.004)
SGLD	1 min	1.001 (0.001)	1.000 (0.004)	0.997 (0.01)	0.989 (0.017)	0.972 (0.028)
	3 min	1.001 (0.001)	1.000 (0.003)	0.998 (0.008)	0.995 (0.013)	0.985 (0.02)
	5 min	1.001 (0.001)	1.000 (0.003)	0.998 (0.006)	0.995 (0.011)	0.990 (0.017)

Table 9: Sensitivity analysis for the stochastic search parameters for the first data generation mechanism ($K = 3$), with $\tau_1 = 1, \tau_2 = 5$. RBODLs for SGEM, SGVI and SGLD under running times of 1, 3 and 5 minutes, with $\kappa = 0.01$ being the reference subsampling ratio. Average RBODL across 50 datasets is shown, with standard deviations in the brackets.

$(\tau_1 = 1, \tau_2 = 0.51)$					$(\tau_1 = 5, \tau_2 = 0.51)$					
methods	RMISE (α, β)	MAE (μ)	IS	ACR	AIW	RMISE (α, β)	MAE (μ)	IS	ACR	AIW
SGLD	0.052 (0.019)	0.109 (0.283)	3.898 (4.739)	0.667 (0.152)	0.844 (0.172)	0.053 (0.014)	0.108 (0.046)	3.912 (3.118)	0.667 (0.129)	0.907 (0.193)
	0.046 (0.008)	0.103 (0.048)	6.163 (2.117)	0.333 (0.131)	0.222 (0.012)	0.046 (0.008)	0.105 (0.048)	6.359 (2.104)	0.333 (0.138)	0.222 (0.012)
SGVI	0.040 (0.007)	0.093 (0.044)	4.905 (1.698)	0.429 (0.139)	0.213 (0.012)	0.040 (0.007)	0.095 (0.044)	4.797 (1.695)	0.429 (0.139)	0.216 (0.012)
	0.049 (0.008)	0.044 (0.042)	-	-	-	0.050 (0.008)	0.046 (0.040)	-	-	-
SGEM	0.046 (0.008)	0.038 (0.037)	-	-	-	0.049 (0.008)	0.044 (0.040)	-	-	-
	0.046 (0.008)	0.038 (0.037)	-	-	-	0.049 (0.008)	0.044 (0.040)	-	-	-

Table 10: Estimation metrics across all seven methods under different sets of stochastic search parameters for the first data generation mechanism ($K = 3$). The values in the grid cells are the average across 50 datasets, with the standard deviation in the brackets.

methods	$(\tau_1 = 1, \tau_2 = 1)$					$(\tau_1 = 5, \tau_2 = 1)$				
	RMISE (α, β)	RMSE(μ)	IS	ACR	AIW	RMISE (α, β)	RMSE(μ)	IS	ACR	AIW
SGLD	0.137 (0.033)	0.264 (0.528)	33.020 (70.245)	0.095 (0.055)	0.231 (0.218)	0.150 (0.033)	0.332 (0.121)	37.133 (66.530)	0.048 (0.056)	0.250 (0.230)
	0.158 (0.024)	0.182 (0.061)	41.842 (12.961)	0.095 (0.046)	0.291 (0.087)	0.158 (0.025)	0.182 (0.061)	41.879 (13.020)	0.095 (0.046)	0.291 (0.088)
SGVI-c	0.152 (0.026)	0.176 (0.061)	36.011 (11.889)	0.095 (0.055)	0.259 (0.070)	0.152 (0.026)	0.176 (0.061)	36.011 (11.889)	0.095 (0.055)	0.259 (0.070)
	0.087 (0.061)	0.136 (0.062)	-	-	-	0.113 (0.061)	0.140 (0.150)	-	-	-
SGEM	0.113 (0.061)	0.147 (0.054)	-	-	-	0.151 (0.043)	0.114 (0.062)	-	-	-

Table 11: Estimation metrics across all seven methods under different sets of stochastic search parameters for the first data generation mechanism ($K = 3$). The values in the grid cells are the average across 50 datasets, with the standard deviation in the brackets.

		RMISE (α, β)	MAE (μ)	IS	ACR	AIW
SGVI-c	$r = 0.5$	0.050 (0.008)	0.097 (0.048)	6.030 (1.420)	0.333 (0.078)	0.220 (0.009)
	$r = 1$	0.040 (0.007)	0.093 (0.044)	4.905 (1.698)	0.429 (0.139)	0.213 (0.012)
	$r = 2$	0.039 (0.007)	0.064 (0.038)	2.609 (1.217)	0.476 (0.097)	0.200 (0.011)
	$r = 3$	0.052 (0.007)	0.077 (0.037)	5.674 (0.770)	0.357 (0.108)	0.180 (0.012)
	$r = 4$	0.080 (0.006)	0.100 (0.045)	13.374 (1.996)	0.238 (0.123)	0.161 (0.012)
	$r = 0.5$	0.050 (0.008)	0.038 (0.040)	-	-	-
SGEM-c	$r = 1$	0.046 (0.008)	0.038 (0.037)	-	-	-
	$r = 2$	0.039 (0.007)	0.024 (0.029)	-	-	-
	$r = 3$	0.048 (0.007)	0.019 (0.025)	-	-	-
	$r = 4$	0.073 (0.007)	0.028 (0.034)	-	-	-

Table 12: Estimation metrics for SGVI-c and SGEM-c under different values of r for the first data generation mechanism ($K = 3$). The values in the grid cells are the average across 50 datasets, with the standard deviation in the brackets.

	MCMC-c	MCMC	SGVI-c	SGVI	SGEM-c	SEM	SGLD
MCMC-c	0.000	0.018	0.302	0.272	0.263	0.252	0.588
MCMC	0.018	0.000	0.294	0.246	0.237	0.228	0.565
SGVI-c	0.302	0.294	0.000	0.294	0.280	0.272	0.485
SGVI	0.272	0.246	0.294	0.000	0.017	0.013	0.565
SGEM-c	0.263	0.237	0.280	0.017	0.000	0.003	0.582
SEM	0.252	0.228	0.272	0.013	0.003	0.000	0.573
SGLD	0.588	0.565	0.485	0.565	0.582	0.573	0.000

Table 13: Mean square distance between the point estimates for α among the seven methods, computed after log transformation.

	MCMC-c	MCMC	SGVI-c	SGVI	SGEM-c	SEM	SGLD
MCMC-c	0.000	0.486	2.385	2.568	2.540	2.596	3.541
MCMC	0.486	0.000	2.596	2.531	2.577	2.577	3.745
SGVI-c	2.385	2.596	0.000	2.373	2.264	2.375	4.290
SGVI	2.568	2.531	2.373	0.000	0.078	0.053	3.435
SGEM-c	2.540	2.577	2.264	0.078	0.000	0.021	3.267
SEM	2.596	2.577	2.375	0.053	0.021	0.000	3.462
SGLD	3.541	3.745	4.290	3.435	3.267	3.462	0.000

Table 14: Mean square distance between the point estimates for β among the seven methods, computed after log transformation.

	MCMC-c	MCMC	SGVI-c	SGVI	SGEM-c	SEM	SGLD
MCMC-c	0.000	0.007	0.090	0.097	0.142	0.129	0.219
MCMC	0.007	0.000	0.114	0.115	0.175	0.161	0.212
SGVI-c	0.090	0.114	0.000	0.061	0.083	0.072	0.270
SGVI	0.097	0.115	0.061	0.000	0.045	0.034	0.324
SGEM-c	0.142	0.175	0.083	0.045	0.000	0.001	0.466
SEM	0.129	0.161	0.072	0.034	0.001	0.000	0.435
SGLD	0.219	0.212	0.270	0.324	0.466	0.435	0.000

Table 15: Mean square distance between the point estimates for μ among the seven methods, computed after log transformation.

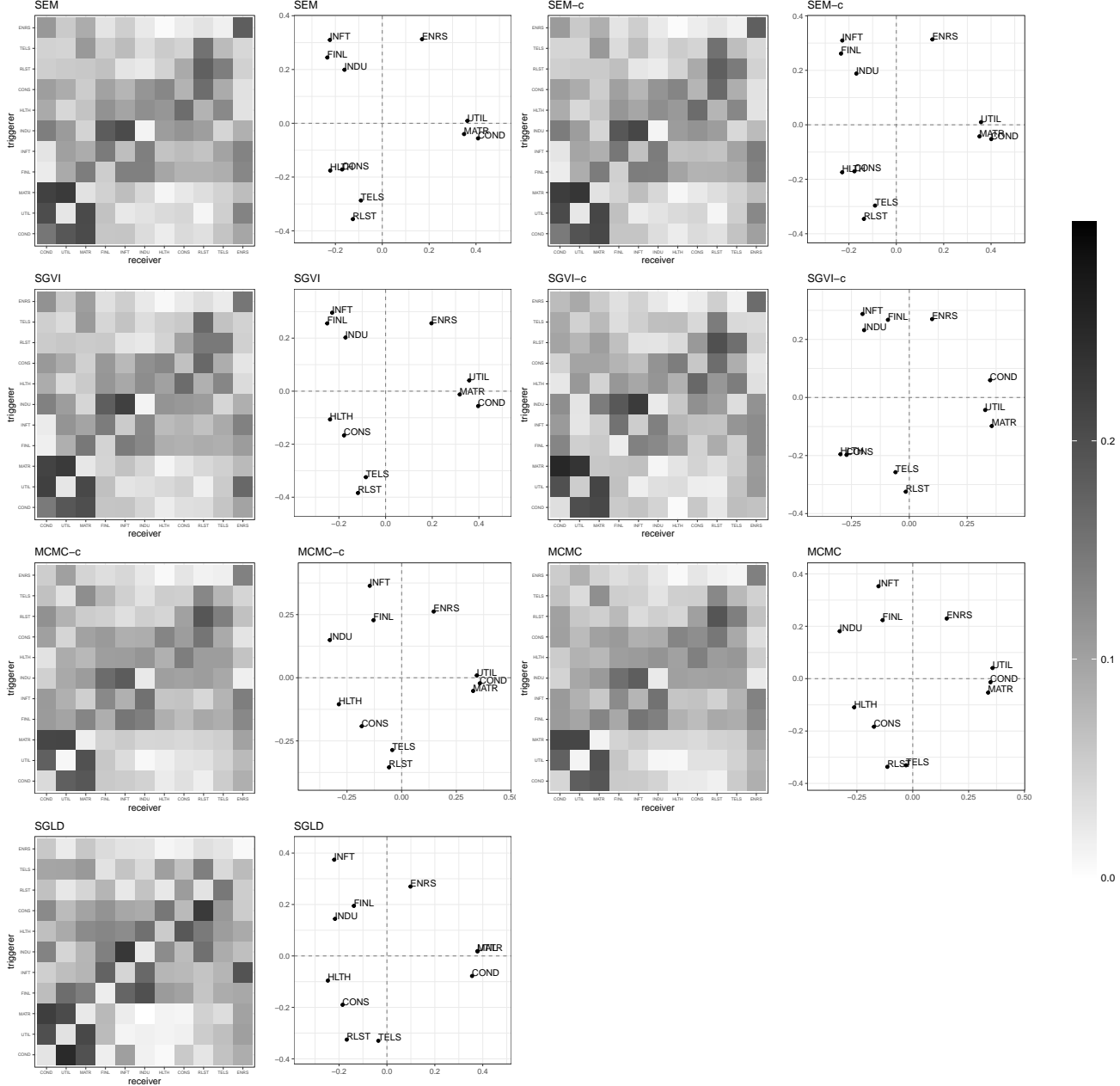


Figure 2: Left panel: heatmaps for point estimates of α parameters for the corresponding 11 sectors, for all seven algorithms. Right panel: first two principal coordinates (after applying the Procrustes analysis algorithm) for the 11 sectors based on the distance measure matrix for α estimates.

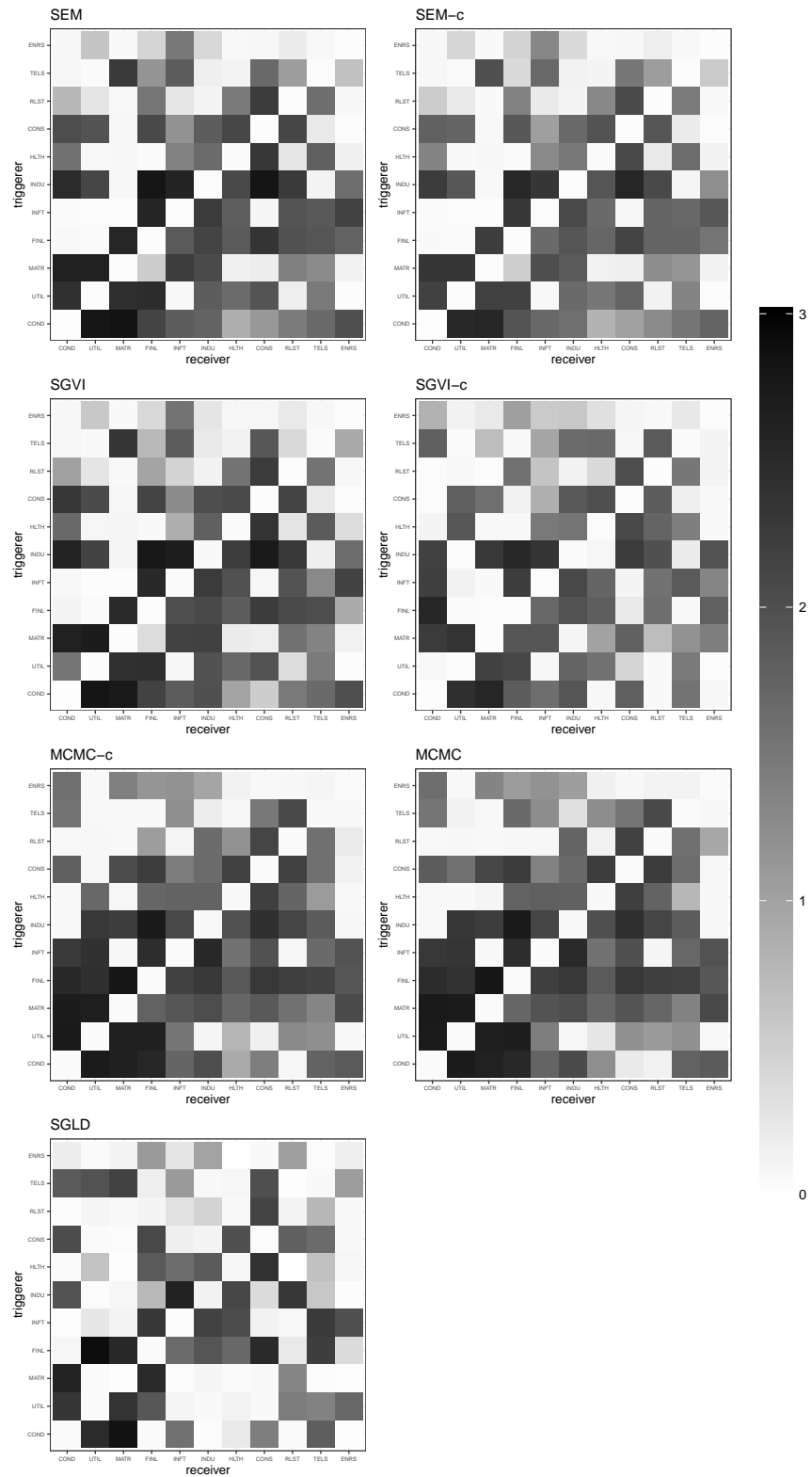


Figure 3: Heatmaps for point estimates of β parameters for the corresponding 11 sectors, for all seven algorithms.

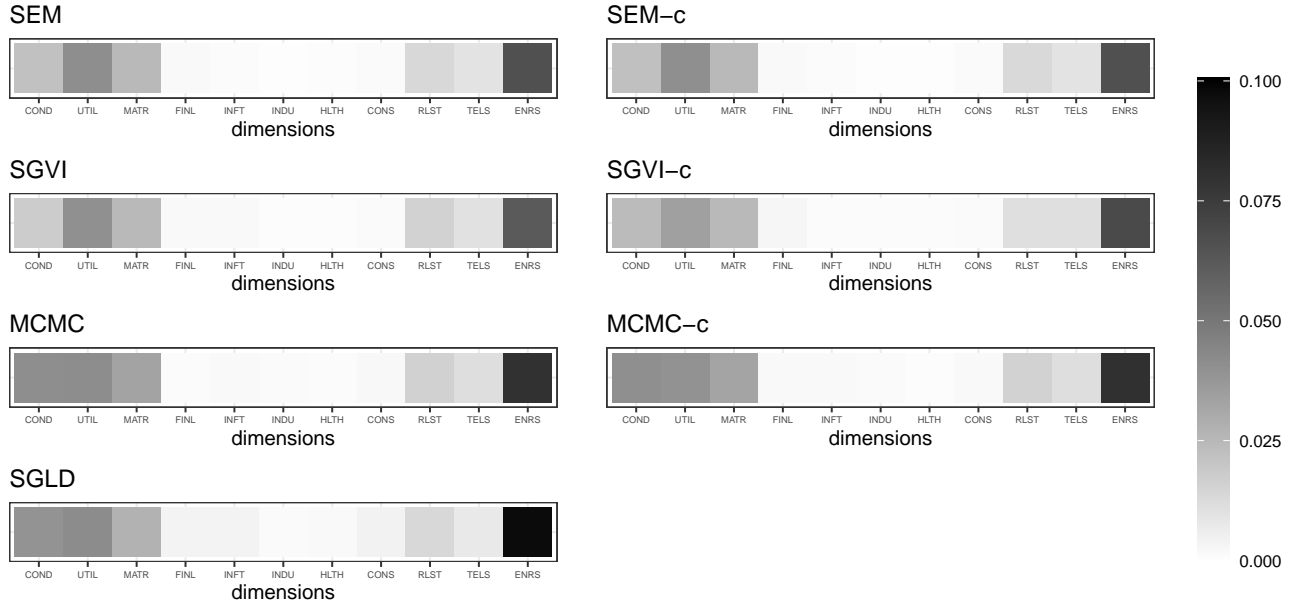


Figure 4: Heatmaps for point estimates of μ parameters for the corresponding 11 sectors, for all seven algorithms.

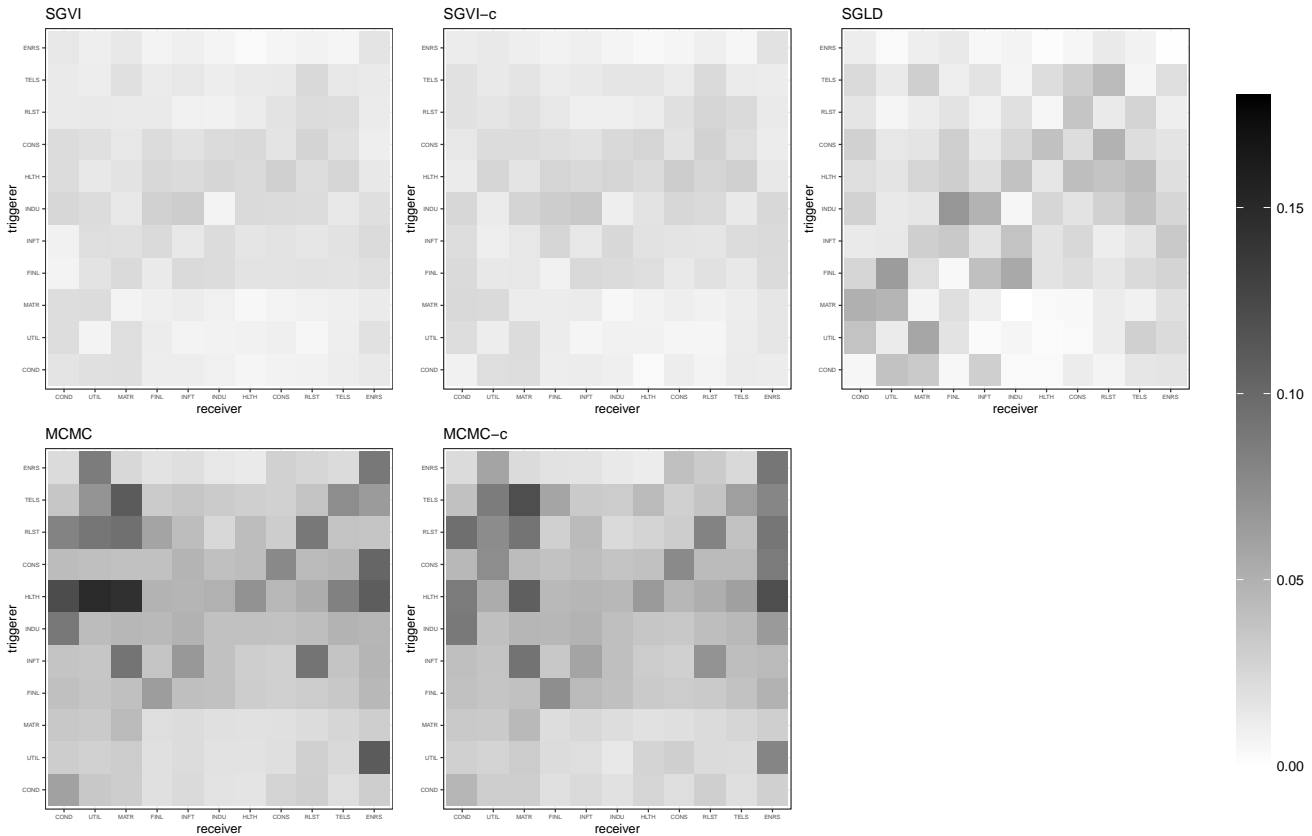


Figure 5: Heatmaps for 95% credible interval lengths estimates of α parameters for the corresponding 11 sectors, for all five algorithms that yield uncertainty estimates.

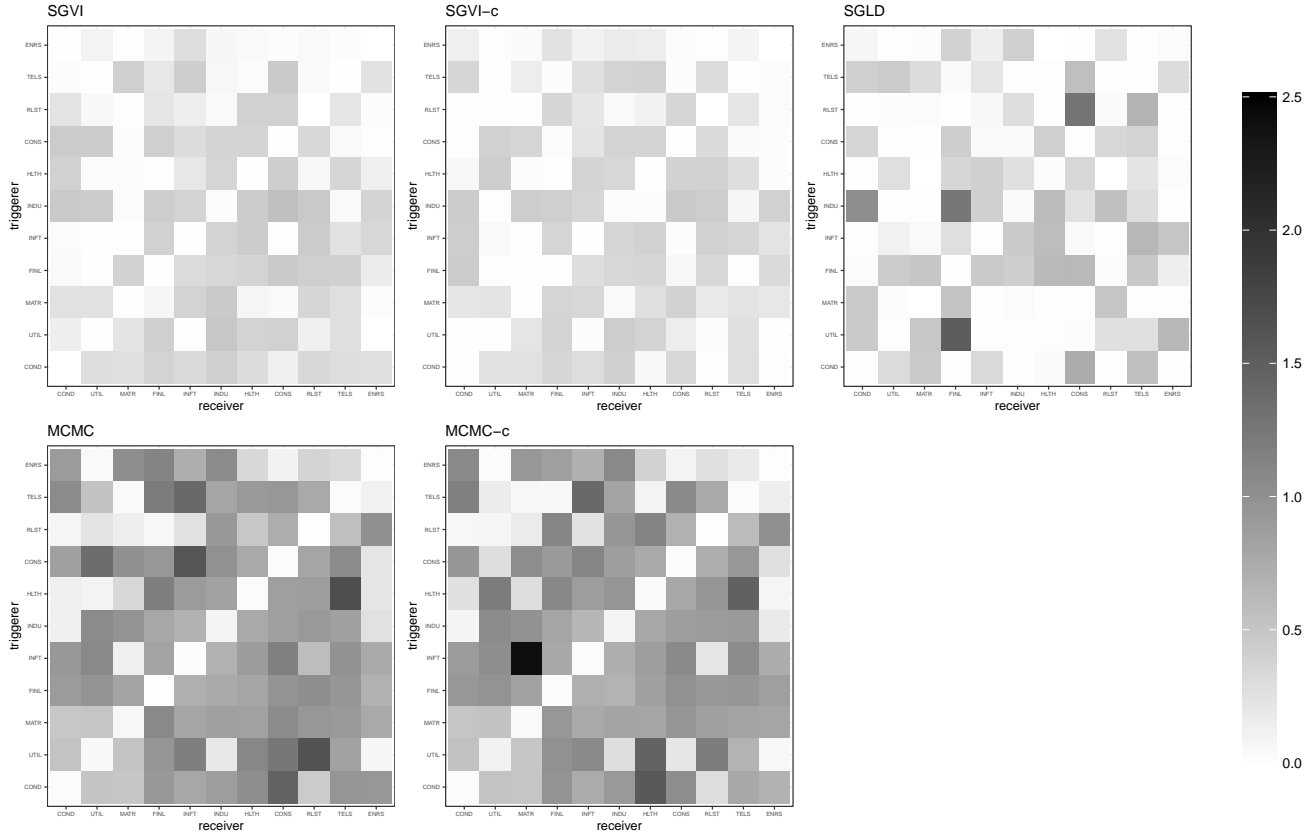


Figure 6: Heatmaps for 95% credible interval lengths estimates of β parameters for the corresponding 11 sectors, for all five algorithms that yield uncertainty estimates.

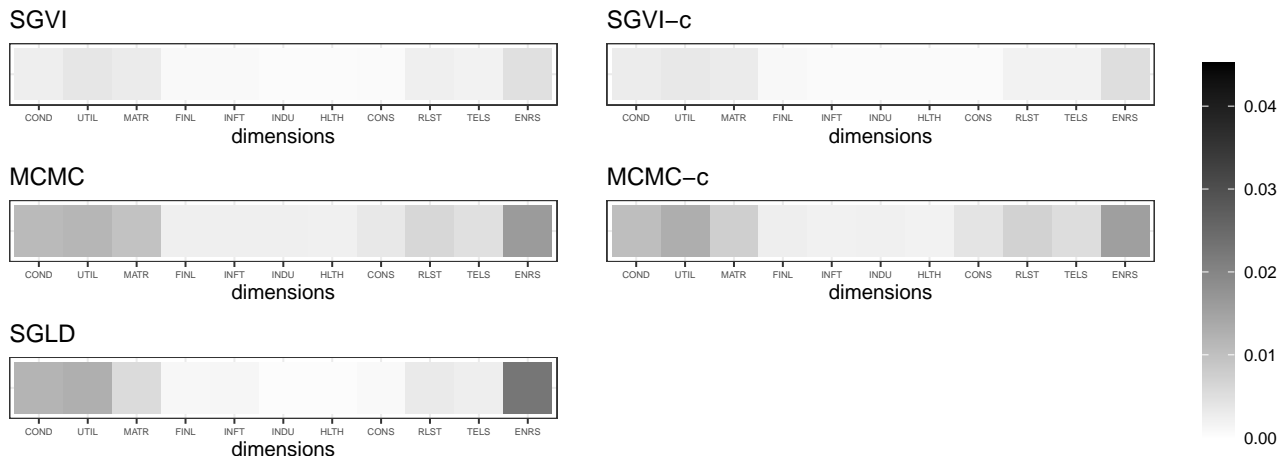


Figure 7: Heatmaps for 95% credible interval lengths estimates of μ parameters for the corresponding 11 sectors, for all five algorithms that yield uncertainty estimates.